

The Effect of Buckling on the Interface Conductance in Flexible Lithium-ion Batteries

A Thesis

Presented to

the Faculty of Department of Mechanical Engineering

University of Houston

In Partial Fulfillment

of the Requirements for the Degree

Master of Science

in Mechanical Engineering

by

Ahmet Akturk

December 2015

The Effect of Buckling on the Interface Conductance in Flexible Lithium-ion Batteries

Ahmet Akturk

Approved:

Chair of the Committee
Haleh Ardebili, Assistant Professor
Mechanical Engineering

Committee Members:

Yashashree Kulkarni, Associate Professor
Mechanical Engineering

Jae-Hyun Ryou, Assistant Professor
Mechanical Engineering

Debora Frigi Rodrigues, Assistant Professor
Civil and Environmental Engineering

Suresh K. Khator, Associate Dean,
Cullen College of Engineering

Pradeep Sharma, Professor, Chair
Department of Mechanical Engineering

Acknowledgements

This thesis and my dreams would not have been fulfilled in both my private and student life without the contribution of a great number of people to whom I cannot express enough thanks. In the beginning, my parents, who brought me into this world, raised me up and always supported, and my brother, with whom I always exchange ideas about everything. Without your support and encouragement, I would not have this opportunity to further my education in the USA.

Now, I would like to express my sincere gratitude to my advisor Dr. Haleh Ardebili for her motivation, nice treatment, continuous support, new ideas, and immense knowledge, for giving me a chance to conduct exciting experiments, for the fruitful discussions throughout my thesis. Her guidance helped me to have productive research and made me learn immense scientific knowledge. It was spectacular to broaden my horizon under the guidance of Dr. Ardebili. Thank you for everything!

I must give my special thanks to the Turkish Government and the Turkish Ministry of Education, who supported me financially and gave me this amazing chance to pursue my Master's degree at the University of Houston. In addition, I would like to thank my thesis committee Dr. Yashashree Kulkarni, Dr. Jae-Hyun Ryou, and Dr. Debora Frigi Rodrigues for their participation as committee members and their dedication and invaluable comments about this thesis.

I am grateful to Mejdi Kammoun, a senior Ph.D student of Dr. Ardebili. Because of his help, I was able to comprehend the fabrication, experiments, and analysis of flexible lithium ion batteries in a timely manner.

I would like to thank all the members of our lab for their positive attitudes. Lastly, I also acknowledge my great roommates and great friends for their full support. Without the people that I mentioned above, I would have never finished this work successfully.

The Effect of Buckling on the Interface Conductance in Flexible Lithium-ion Batteries

An Abstract

of a

Thesis

Presented to

the Faculty of Department of Mechanical Engineering

University of Houston

In Partial Fulfillment

of the Requirements for the Degree

Master of Science

in Mechanical Engineering

by

Ahmet Akturk

December 2015

Abstract

Flexible batteries used in flexible applications including medical implants, wearable electronics, consumer electronics or roll-up displays are often subjected to bending and buckling during their operation life. It is imperative to investigate the impact of buckling on the performance of the flexible lithium ion battery (LIBs). In this study, flexible thin-film lithium ion batteries based on solid nanocomposite polymer electrolyte were fabricated. The interfacial impedance in fresh and cycled flexible LIBs was investigated in flat and buckled configurations using electrochemical impedance spectroscopy (EIS). It is demonstrated that with increasing value of curvatures, contact resistances between components can be reduced and contact conductance of LIBs can be enhanced.

Table of Contents

Acknowledgements	iv
Abstract	vii
Table of Contents	viii
List of Figures	xi
List of Tables	xiv
Chapter 1 Introduction	1
1.1 Lithium-ion Batteries	1
1.2 Flexible Lithium-ion Batteries	4
1.3 Buckling and Bending Mechanics.....	10
1.4 Electrochemical Impedance Spectroscopy for Impedance Measurement of Lithium-ion Batteries	14
Chapter 2 Experiments.....	21
2.1 Overview	21
2.2 Materials.....	21
2.3 Equipment	23
2.4 Fabrication Process	26
2.4.1 Preparation of Solid PEO (100,000 Mw)/GO/LiClO ₄ Electrolyte	27
2.4.2 Preparation of Solid PEO (600,000 Mw)/GO/LiClO ₄ Electrolyte	28

2.4.3	Preparation of Current Collectors and Electrodes	29
2.4.4	Fabrication of Flexible Lithium-ion Battery.....	29
2.5	Characterization	31
2.5.1	Capacity Measurement.....	32
2.5.1.1	Capacity Measurement at Room Temperature.....	33
2.5.1.2	Capacity Measurement at High Temperature	34
2.5.2	Buckling/Bending Analysis.....	34
2.5.3	Electrochemical Impedance Spectroscopy	36
2.5.3.1	Nyquist Plots and Circuit Modeling	39
Chapter 3	Results and Discussions	43
3.1	Fabricated Flexible Lithium-ion Batteries	43
3.2	Electrochemical Characterization of Flexible LIBs	46
3.3	Nyquist Plots of Fresh and Cycled Lithium Ion Batteries	48
3.3.1	Nyquist Plots of Fresh Batteries	48
3.3.2	Nyquist Plots of Cycled Batteries	51
3.3.3	Nyquist Plots of Other Cycled Batteries.....	54
3.3.4	Nyquist Plots of Batteries Cycled at 50 °C	58
3.4	Fit and Simulation-Based Equivalent Circuits of Fresh and Cycled Batteries ..	60
3.5	Resistance and Conductance at Different Buckling Curvatures	66
3.5.1	Total Resistance and Total Conductance for Different curvatures	66

3.5.2	Normalized Contact Conductance for Different Curvatures	71
Chapter 4 Conclusions and Future Work.....		77
4.1	Conclusions	77
4.2	Future Work	79
References.....		82

List of Figures

Figure 1.1 Volumetric and gravimetric energy densities of different kind of batteries.....	2
Figure 1.1 The Mechanism of Lithium-ion batteries.....	3
Figure 1.3 Layers of flexible Lithium-ion batteries.....	6
Figure 1.4 Four different buckling cases with the effective lengths.....	11
Figure 1.5 The Mechanism of three-point bending and four point-bending.....	13
Figure 1.6 Sinusoidal current response to the applied potential and phase shift.....	15
Figure 1.7 General Nyquist plot of fresh LIBs.....	17
Figure 1.8 General Nyquist plot of cycled LIBs.....	18
Figure 2.1 Glove box system.....	25
Figure 2.2 Vacuum Oven.....	25
Figure 2.3 Preparation of the solid nanocomposite electrolyte.....	28
Figure 2.4 Fabricated flexible LIB powering an LED and layers of flexible LIB.....	30
Figure 2.5 Double lamination process of the battery.....	31
Figure 2.6 Capacity measurement procedure.....	33
Figure 2.7 The buckling test and determining curvatures with circle fitting method.....	35
Figure 2.8 The frequency scan parameters.....	37
Figure 2.9 FRA potentiostatic procedure.....	38
Figure 2.10 The equivalent circuit used for fitting of nyquist plot of a fresh battery.....	40
Figure 2.11 The equivalent circuit used for fitting of nyquist plot of cycled battery.....	41
Figure 3.1 Fabricated flexible LIB powering the red LED.....	44
Figure 3.2 Flexible batteries at flat position and at three different curvatures.....	44
Figure 3.3 The fabricated battery at three different curvatures and angles	45
Figure 3.4 The nanocomposite solid polymer electrolyte.....	45

Figure 3.5 Specific capacities of Battery 1, Battery 2 and Battery 3 based on 100,000 Mw PEO at room temperature.....	46
Figure 3.6 Specific capacities of Battery 4, Battery 5 and Battery 6 based on 600,000 Mw PEO at room temperature	47
Figure 3.7 Specific capacities of Battery 7, Battery 8 and Battery 9 based on 100,000 Mw PEO at 50°C.....	47
Figure 3.8 Nyquist plots of fresh battery 1 at different curvatures.....	48
Figure 3.9 Nyquist plots of fresh battery 2 at different curvatures.....	49
Figure 3.10 Nyquist plots of fresh battery 3 at different curvatures.....	50
Figure 3.11 Nyquist plots of cycled battery 1, fabricated using an electrolyte prepared with 100,000Mw PEO host.....	51
Figure 3.12 Nyquist plots of cycled battery 2, fabricated using an electrolyte prepared with 100,000Mw PEO host.....	53
Figure 3.13 Nyquist plots of cycled battery 3, fabricated using an electrolyte prepared with 100,000Mw PEO host.....	54
Figure 3.14 Nyquist plots of cycled battery 4, fabricated using an electrolyte prepared with 600,000Mw PEO host.....	55
Figure 3.15 Nyquist plots of cycled battery 5, fabricated using an electrolyte prepared with 600,000Mw PEO host.....	56
Figure 3.16 Nyquist plots of cycled battery 6, fabricated using an electrolyte prepared with 600,000Mw PEO host.....	57
Figure 3.17 Nyquist plots of battery 7, fabricated using an electrolyte prepared with 100,000Mw PEO host and cycled in the oven.....	58
Figure 3.18 Nyquist plots of battery 8, fabricated using an electrolyte prepared with 100,000Mw PEO host and cycled in the oven.....	59
Figure 3.19 Nyquist plots of battery 9, fabricated using an electrolyte prepared with 100,000Mw PEO host and cycled in the oven.....	60
Figure 3.20 The equivalent circuit used to fit measured data of fresh batteries.....	61
Figure 3.21 The equivalent circuit used to fit measured data of cycled batteries.....	61
Figure 3.22 Total resistance of fresh batteries.....	66

Figure 3.23 Total conductance of fresh batteries.....	67
Figure 3.24 Total resistances of cycled Batteries 1, 2 and 3.....	67
Figure 3.25 Total conductance of cycled Batteries 1, 2 and 3.....	68
Figure 3.26 Total resistances of cycled Batteries 4, 5 and 6.....	69
Figure 3.27 Total conductance of cycled Batteries 4, 5 and 6.....	69
Figure 3.28 Total resistances of cycled Batteries 7, 8 and 9.....	70
Figure 3.29 Total conductance of cycled Batteries 7, 8 and 9.....	70
Figure 3.30 Normalized contact conductance of fresh battery 1, battery2 and battery 3 at different curvatures	71
Figure 3.31 Normalized contact conductance of battery 1, battery 2 and battery 3 cycled at room temperature and tested at room temperature under different buckling curvatures.....	72
Figure 3.32 Normalized contact conductance of batteries using an electrolyte prepared with 600,000 Mw PEO, cycled at room temperature and tested at room temperature under different buckling curvatures.....	73
Figure 3.33 Normalized contact conductance of batteries cycled at 50°C and tested at room temperature under different buckling curvatures.....	74
Figure 3.34 Plot of the average contact pressure change with increasing curvature based on the numerical study conducted by Sean Berg.....	75

List of Tables

Table 2.1 Material properties of current collectors, electrodes and current conductors.....	22
Table 2.2 Materials used in the preparation of solid polymer electrolyte.....	23
Table 2.3 Equipment used in experiments.....	24
Table 2.4 Properties of components used in the fabrication of the battery.....	30
Table 3.1 The EC elements with their values for fresh batteries, fabricated using an electrolyte prepared with 100,000Mw PEO host.....	62
Table 3.2 The EC elements with their values for batteries, fabricated using an electrolyte prepared with 100,000Mw PEO host and cycled at room temperature.....	63
Table 3.3 The EC elements with their values for batteries, fabricated using an electrolyte prepared with 600,000Mw PEO host and cycled at room temperature.....	64
Table 3.4 The EC elements with their values for batteries, fabricated using an electrolyte prepared with 100,000Mw PEO host and cycled at 50 °C.....	65

Chapter 1 Introduction

1.1 Lithium-ion Batteries

Due to the depletion of nonrenewable energy sources, increasing demand for fossil fuels and the need for clean energy to prevent global warming and climate changes, there is an increasing interest for new energy sources [27]. Renewable energy sources alternative to fossil fuels that derive from the water stored in the dam, or the sun, the wind or the water waves are often intermittent and can benefit high efficiency energy storage systems. The electrochemical storage devices in the form of batteries which can store and deliver energy play an important role in meeting the requirements of high efficiency energy storage systems and not only they benefit the aforementioned intermittent power sources, but they are also used to directly power the consumer electronics (i.e., laptops, cell phones, etc.), transportation, and aerospace applications [20, 27]. The characteristics of batteries are mainly determined by the materials used for the battery components. Being the third lightest element after hydrogen and helium, and the lightest element among metals, lithium takes the form of Li^+ by ionization and can carry and move the positive charge in a very small distances. Therefore, lithium has excellent electrochemical properties which makes it a perfect material for developing a relatively higher energy and power density battery [27]. Lithium-ion batteries (LIBs) have been widely applied on many devices and systems for decades, and are one of the most outstanding candidates for power sources due to their high energy density, long-term stability, and the ability to be recharged many times with slow capacity fading compared to other rechargeable batteries [12].

Figure 1.1 shows that the lithium-ion battery (LIB) has a clear advantage of much higher power and energy density compared to its predecessors, namely, nickel-metal-hydride (NiMH), nickel-cadmium (NiCd) and lead-acid batteries [29]. A typical conventional LIB is comprised of graphite anode (with specific capacity of 300–350 mAh g⁻¹), lithium metal oxide cathode (e.g., LiMO₂, M=Co, Ni, Mn, with specific capacity of 140–160 mAh g⁻¹) and an electrolyte and separator which must be ionically conductive and electrically insulating [18]. As depicted in Fig 1.1, lithium metal batteries have the highest specific power and specific energy. However, dendritic growth of lithium through the electrolyte, short circuits and internal heating which create serious safety and stability concerns are the main issues with lithium metal batteries that caused the removal of Li-metal batteries from the market in the late 1980s [27].

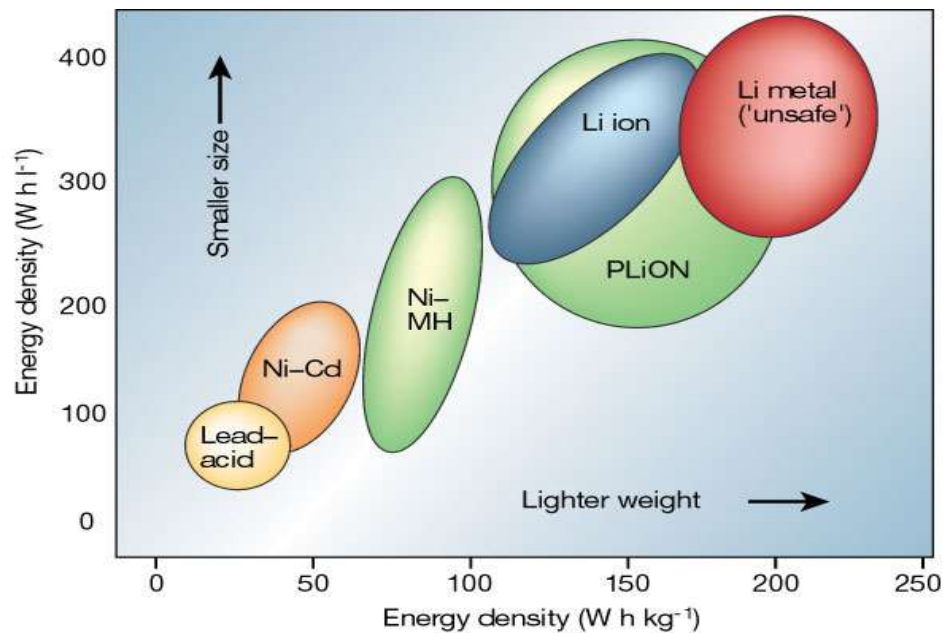


Figure 1.1 Volumetric and gravimetric energy densities of different kind of batteries [29].

During the charging process, the general working principle of lithium ion batteries is as the following: The positively charged lithium ions move through the electrolyte from the positive electrode (cathode) to the negative electrode (anode) where they are stored. The electrons, on the other hand, move through the external circuit from the cathode to the anode. During discharge, the electrochemical process and direction are reversed and a usable external electrical circuit is generated.

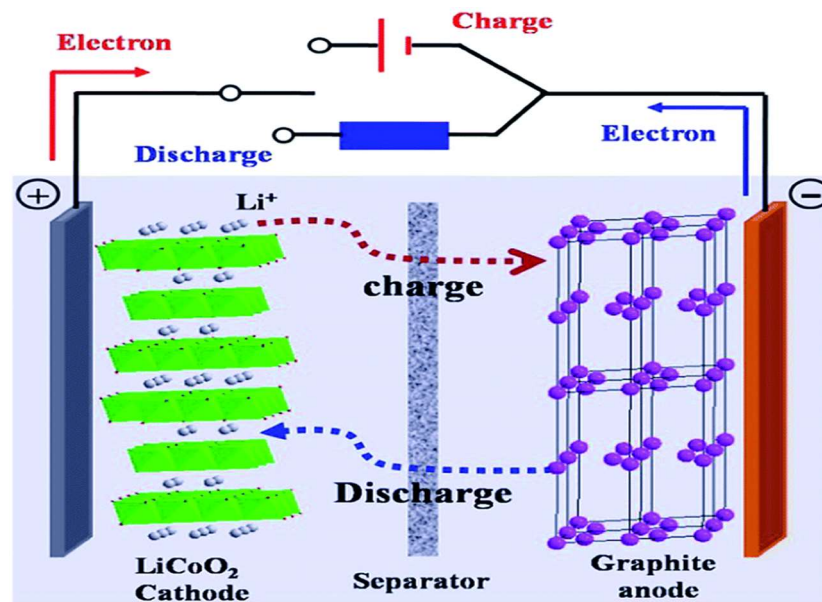
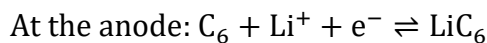
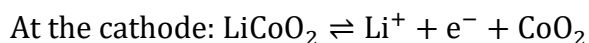


Figure 1.2 The mechanism of lithium-ion batteries [30].

During the charging of flexible lithium ion batteries, oxidation and de-lithiation occur in LiCoO_2 cathode. Simultaneously, reduction and lithiation take place in the graphite anode. During the battery discharge, the processes are reversed [34]. The charge (\rightarrow) and (\leftarrow) discharge chemical reactions are shown below:



As seen from the reactions, LiC_6 forms as the final byproduct after the intercalation of graphite with lithium ions and this is a reversible process [34]. Safety, reliability, cost, lifetime and power are some of the most important parameters in LIBs. For future designs and applications, higher performance and cost-efficient LIBs can be produced by the modification or replacement of graphite and lithium cobalt oxide with higher capacity, lower cost anode and cathode materials. Also, electrolyte can be more reliable, safer and more ionic conductive [18].

1.2 Flexible Lithium-ion Batteries

A flexible electronic device must ideally function under buckling, bending, stretching, compression, twisting and deformation into arbitrary shapes and it should also accommodate relatively large strain deformation greater than 1% [7, 12, 15]. Improvements in flexible electronics have become ever-increasingly crucial to the cutting-edge technology. Although some evolution of mechanically flexible electronic devices has taken place, their suitability has been bounded by limited applications, such as light-emitting diodes (LEDs), sensing electrodes, circuit elements, and radio frequency identification (RFID) antennas [9]. Flexible electronics have the potential to revolutionize an industry and to lead to new designs [4]. Flexible power supplies are now widely in demand for integration with flexible electronics [2]. There is an increasing affinity in high-performance, thin and lightweight flexible power sources to fulfill the special designs and features for new-generation electronics such as bendable, soft and portable electronics, roll-up displays, wearable devices, implantable biomedical devices, and conformable health-monitoring electronic skin [9, 11].

Since 1990s, lithium-ion batteries (LIBs) have been widely applied in portable devices, and are one of the most outstanding candidates of power sources for flexible devices due to their large energy density, high power density, and long service life compared to other batteries [6, 12]. Flexible lithium ion batteries (LIBs) can make significant contribution as a vital component to guide future flexible electronic devices [12]. The primary challenge is not only manufacturing of batteries, but also the stability of these devices in terms of mechanical, electrical, or electrochemical properties [1]. Reliable safety, high electron and ion conductivity, vigorous mechanical flexibility, and distinguished corrosion resistance is aimed to be successful in flexible LIBs [11]. The numerical and experimental studies are important to determine resilience of complete flexible electronics and flexible energy storage devices. Since bendable or wearable batteries are flexible materials, it is really critical that flexible materials be tested under buckling or bending conditions. Components of flexible systems like LIBs must be still deformable and functional in application have robust mechanical flexibility. In addition, under deformation, mechanical properties of different components of flexible batteries must be compatible. By deforming flexible, thin, lightweight lithium ion battery, failure of battery and change in performance can be investigated. Electrodes and the electrolyte are the most important components of LIBs. The interface contact between the electrodes and the electrolytes of the LIBs has a vital importance for stable operation. With repeated buckling, bending and stretching, the electrolyte must be flexible and must have stable contact with the electrodes [12]. Materials currently used in conventional LIBs are limited. Therefore, what could be used in flexible batteries is not many but certain materials.

Components of conventional LIBs (electrode, separator, and electrolyte) need to be either modified or replaced by new materials to be used in flexible battery and to be functional during mechanical deformation [6, 12]. Figure 1.3 shows example of thin layers used to fabricate flexible lithium ion battery.

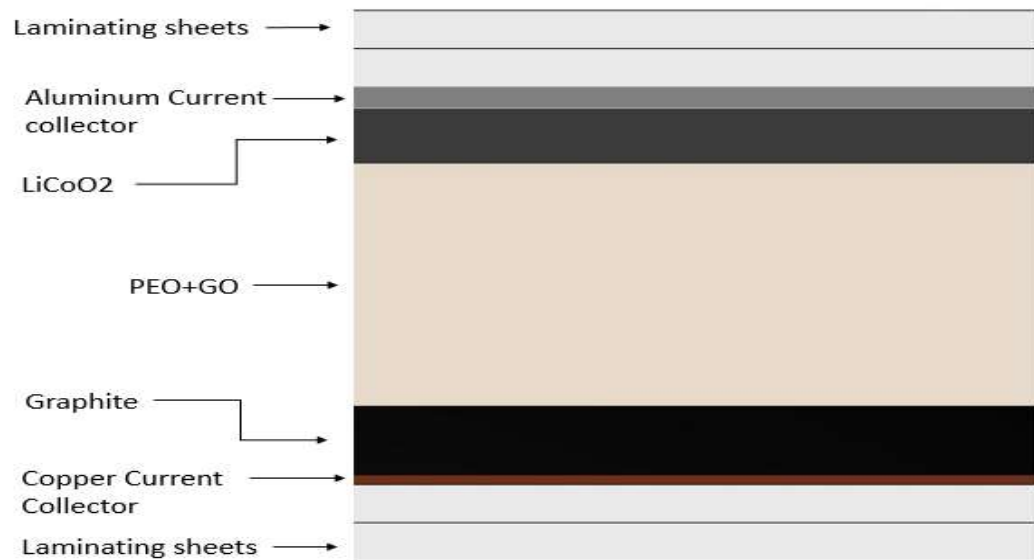


Figure 1.3 Layers of flexible Lithium-ion batteries.

During the development of flexible batteries, current collectors must be handled with care because they can impact the performance of the flexibility of battery and can affect the mechanical properties of the entire battery. Along this direction, in LIBs, due to their decent mechanical strength and high conductivity, aluminum and copper have been operated as the current collectors [6, 12]. Bendable and stretchable current collectors can be achieved by using thin copper and aluminum sheets as current collectors or different flexible and stretchable materials can be used as current collectors such as textiles. Without having bendable and electrochemically active electrodes, the assembly of the conventional LIBs cannot correspond to flexible batteries.

For the satisfactory operation of flexible LIBs, the electrodes can be tested under different buckling modes, forces and compressive stresses to make sure that no crack forms and that their mechanical strength is robust enough. Recently, carbon nanotubes (CNTs) and graphene and their composites due to the high charge-carrier mobility, polymer electrodes such as Polyaniline (PANI) and Polyrrole due to their mechanical flexibility, mixtures of nanostructured active materials, carbon nanofibers and metal oxide-based nanowires have been reported as electrodes for flexible LIBs [9]. Although, their suitability, versatility, and mechanical flexibility make them good candidate for flexible LIBs, electrochemically active polymers have lower electrochemical stability, lower energy density, lower power density and poor conductivity [12]. In addition, by utilizing the advantages of at least two components, composite electrodes can be taken into consideration due to their high capacity, mechanical flexibility and cyclic stability under buckling, bending, stretching or deformation [14]. Typically, the surface area of the pores in the electrode material can highly impact the capacity of the LIBs. Hence, advanced discharge and charge capacity can be reached by choosing a highly porous material with a large pore diameter [10]. The resistivity of the electrode which is the resistance of the material to the flow of an electric current could affect the performance of flexible LIBs significantly. The resistivity of the two electrodes in the flexible battery must be measured and evaluated separately under buckling and in flat position [2]. The particular electrical failure in the flexible electronics by the repeating deformation continues to be one of the many reliability issues considering that the interconnections of each surface between each flexible layer experience bending, stretching, and twisting throughout their usage. Any fracture or repeated deformations in the interface or bulk of the LIB components during buckling can result in severe electrical resistance rise [13].

Furthermore, buckling of LIBs can deteriorate the retention capacity during the charge and discharge cycles [9]. The capacity of the battery should be stable and the capacity fading should be avoided after certain cycles for a promising electrochemical performance.

Electrolyte is another essential element of the flexible batteries that influences the electrochemical behavior of battery and plays a vital role in the transportation of ions between two electrodes, as well as preventing direct electrical contact of the two electrodes (i.e., electrical shorting). Interface property of the electrolyte is one of the key components of the performance of flexible batteries, as the electrolyte transports ions from one electrode towards another. The impedance of a battery is associated with several factors, among which is the ionic conductivity of electrolyte. Higher ionic conductivity of the electrolyte, leads to better Li ion transport and lower impedance [12]. Liquid, solid and gel electrolytes are used in different types of batteries. The liquid electrolytes have disadvantages of solid electrolyte interphase (SEI), dendrite growth, thermal runaway and, liquid electrolytes may cause internal-short circuits, leakage and catastrophic fire hazards under serious mechanical distortion [17]. Gel-polymer electrolytes (GPEs) offer good mechanical flexibility and moderate ionic conductivity and enhanced safety compared to organic liquid electrolytes. These properties makes GPEs one of the most commonly used electrolyte in flexible battery [12]. However, the mechanical stability of GPEs is still an issue. Solid polymer electrolytes (SPEs) resolve the concerns in terms of reliable safety because of their suppression of dendrite growth, and higher thermal, electrochemical stability. Furthermore, SPEs can be manufactured as thin films to use in flexible batteries. Therefore, SPEs like solid polyethylene oxide (PEO) are excellent candidates for flexible LIBs.

However, SPEs low ionic conductivity of SPEs especially at room temperature is the main issue to overcome [17]. Various ceramic fillers nanofillers such as Al_2O_3 , SiO_2 , LiAlO_2 , and TiO_2 with polymer host has shown enhancement in ionic conductivity of SPEs. Incorporation of graphene oxide nanosheets in the PEO host has attracted attention due to its high ionic conductivity and high tensile strength [17]. For flexible batteries, under buckling, bending or twisting, undesirable plastic deformation may be observed in solid electrolytes. It is critical that the solid electrolyte used in a flexible battery design does not exhibit plastic deformation up to certain desirable curvature. Failure limits of each layer in the LIBs must be identified and analyzed because multi-layered-flexible battery may fail due to the failure in even one layer of stack. Furthermore, the interaction, adhesion and cohesion among layers is another important parameter to be fully understood [4]. Methods of combination, application and fabrication of the electrodes, electrolytes, and separators into a device influence the electrochemical and mechanical properties of the LIBs. Failure of layered materials also include micro cracks and fraction under stress. Pre-existing defects, scratches and edge defects can cause early failure of the multi-layered structure. As a consequence of repeated buckling or bending, stable interface between electrodes and current collectors can be deteriorated by interfacial delamination and failure can occur [3]. By preventing these undesirable failures and minimizing such defects, it is possible to have better capacity and performance even in the case of high buckling and bending curvatures.

1.3 Buckling and Bending Mechanics

Buckling is a phenomenon that can suddenly cause structures to be unstable or to have a large deformation under compressive loads or stresses. Due to buckling, a structure or its components tend to fail even at much smaller loads than those which cause failure of structures [36]. Generally, an axis which has minimum area moment of inertia accommodates buckling. The critical buckling load (P_{cr}) is the lowest load at which buckling may occur. It is given by

$$P_{cr} = \frac{\pi^2 EI}{L^2}, \quad (1)$$

where P_{cr} is critical force (lb , N), I is area of moment of inertia (in^4 , m^4), E (lb/in^2 , Pa (N/m^2)) is elastic modulus and L (in, m) is effective length of structure [36]. For the flexible lithium ion batteries, different buckling modes can be used to analyze structure of the battery and mechanical stability of whole system. Also, various bending methods can be helpful to investigate structural failure of the flexible electronics. When a thin component is bent, the tensile stress is active on the outer surface and the compressive stress is present at the inner surface. Under tensile or compressive strain, the resistance of materials can increase or decrease depending on the circumstances and inherent material properties [5]. While high strain can cause serious electrical and mechanical problems, low strain usually does not lead to any damage on material [13]. Choosing suitable material and suitable thickness, strain can be modulated better or decreased [8]. The reason to test battery under different buckling modes and bending methods is to observe compatibility of battery to the different applications.

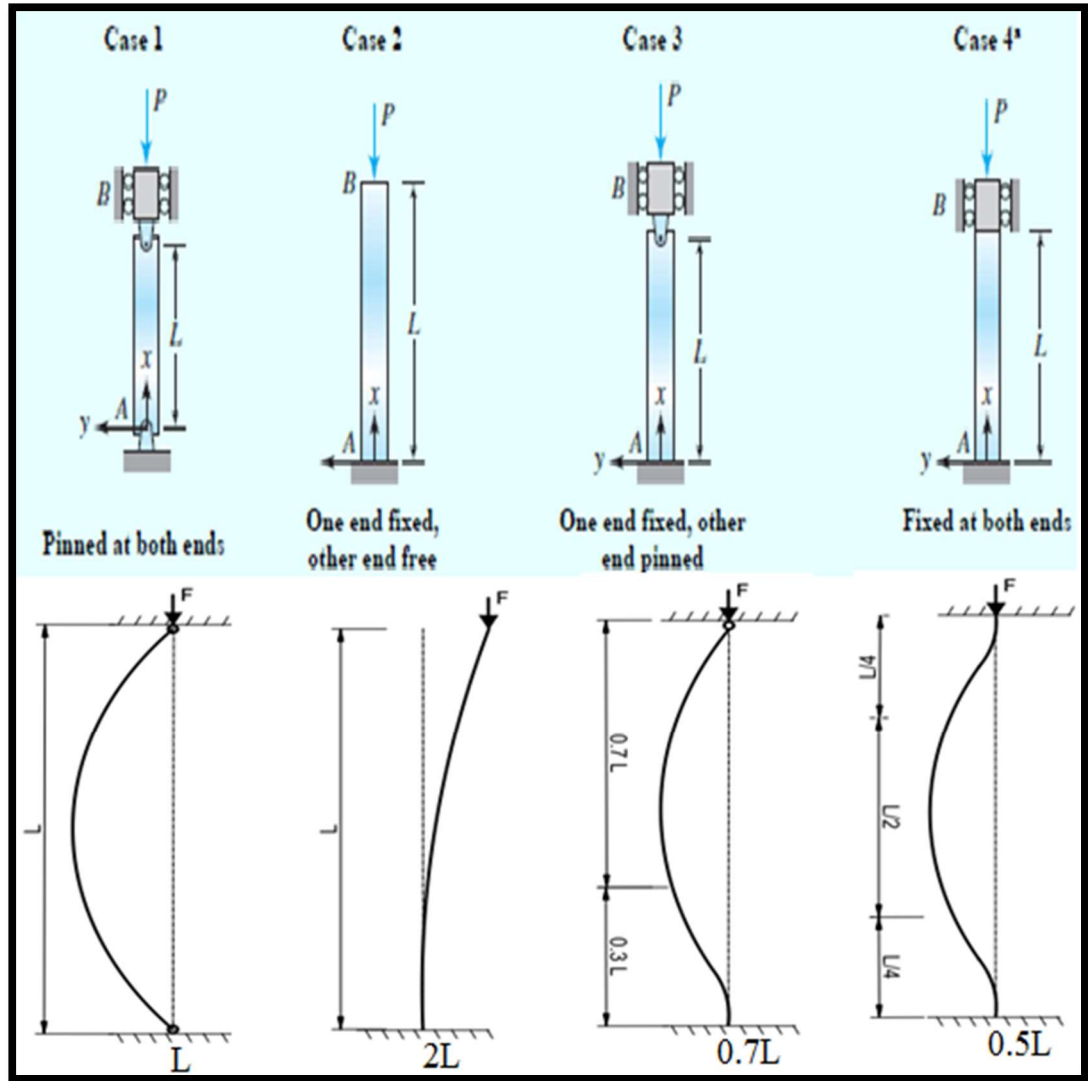


Figure 1.4 Four different buckling cases with the effective lengths [36, 37].

Figure 1.4 shows four different buckling cases based on the end support types and different effective lengths for the first mode buckling. The flexible batteries investigated in this study were subjected to Case 4-first mode buckling. Assuming an effective length of L , the critical force for the structure pinned at both ends is given by

$$P_{cr} = \frac{\pi^2 EI}{L^2}. \quad (2)$$

For the structure that has one fixed end and one free end, the critical force can be calculated by

$$P_{cr} = \frac{\pi^2 EI}{(2L)^2} = \frac{0.25\pi^2 EI}{L^2}. \quad (3)$$

For the structure that has one fixed end and one pinned end, the critical force yields Equation 4 given by

$$P_{cr} = \frac{\pi^2 EI}{(0.7L)^2} = \frac{2.04\pi^2 EI}{L^2}. \quad (4)$$

For the structure that has one fixed end and one pinned end, the critical force can be calculated by

$$P_{cr} = \frac{\pi^2 EI}{(0.5L)^2} = \frac{4\pi^2 EI}{L^2}. \quad (5)$$

In Figure 1.5 the principle three-point bending and four-point bending is displayed. For both bending models, the material parameters and the thickness of the specimen plays a key role to determine the amount of bending. The maximum stress in a structure is an important parameter for design and analysis. For the four-point bending, the stress is at maximum in the region between the supports. For the three-point bending, the maximum stress occurs at the point where the force is applied [1].

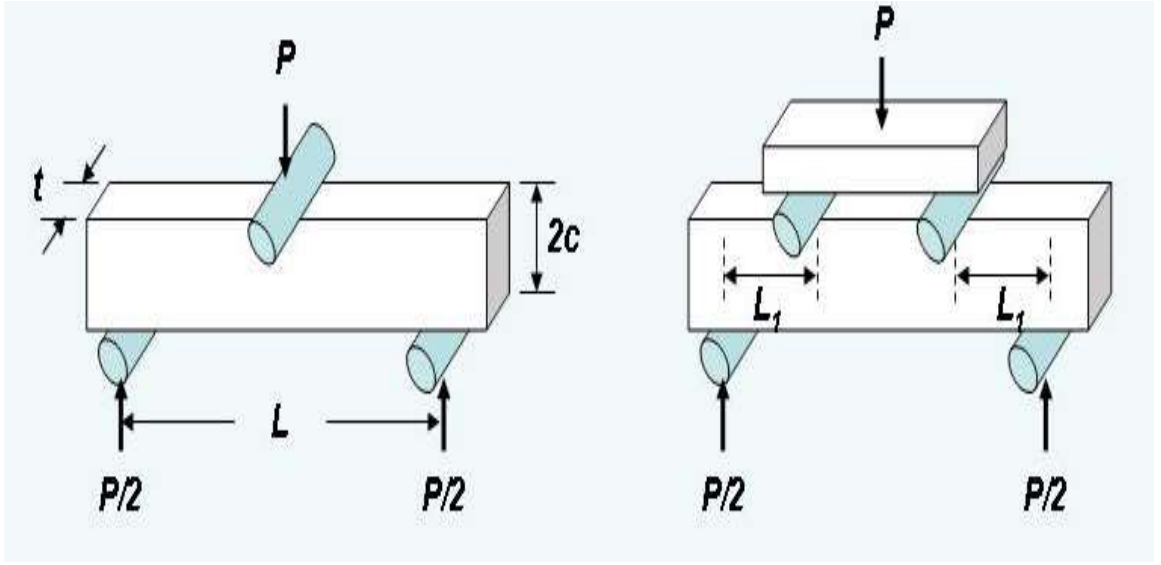


Figure 1.5 The mechanism of three-point bending and four point-bending [38].

Under the three-point bending, the length L between the two rollers is used to calculate the maximum stress. The maximum bending stress located at the outer surface (furthest from the neutral axis) is given by

$$\sigma = \frac{3PL}{2wt^2}, \quad (6)$$

where t is the thickness, w is the width of structure and P is the applied force [38].

According to the Bernoulli–Euler beam equation, the maximum stress for the four-point bending is expressed by

$$\sigma = \frac{3PL_1}{wt^2}, \quad (7)$$

where P is the applied force, w is the width of the specimen which is equal to $2c$, t is the thickness of the specimen and L_1 is the distance between the inner one inner support and one outer support [39].

The maximum strain for the three-point bending test can be calculated by

$$\varepsilon = \frac{3PL}{2Ewt^2} . \quad (8)$$

The maximum strain for the four-point bending test can be calculated by

$$\varepsilon = \frac{3PL}{4Ewt^2} . \quad (9)$$

L is the undeformed length of specimen, w is the width of specimen, t is the thickness of the specimen and E is the flexure modulus.

1.4 Electrochemical Impedance Spectroscopy for Impedance Measurement of Lithium-ion Batteries

Battery behaviors at all operational conditions must be known accurately in order to achieve high performance. The diverse processes inside the cell must be measured as well as interpreted to acquire in-depth knowledge of the battery mechanisms.

Electrochemical impedance spectroscopy (EIS) is a reliable electro-analytical way of characterizing the kinetics inside different types of power sources [21]. The impedance of each kinetic step during each reaction in the power sources can be obtained by EIS. EIS have been utilized to study lithium-ion (Li-ion) batteries for many years. EIS enables the discovery of the actual processes that limit the battery performance and provides remarkable predictive capabilities pertaining to the optimization of the battery design. Impedance characteristics of battery plays an important role to determine power capability and the ability of the battery to deliver a certain power.

Impedance of storage devices is affected by the current, the previous history, temperature and state-of-charge (SoC) that tests are completed upon the change of the impedance at various depths of charge and discharge in a certain cycles for investigation of the reaction mechanism and kinetics. In addition, impedance characteristics are also influenced by the battery life time such as aging [25, 26]. EIS method is based on the principle which sinusoidal signal at a given frequency is generated and imposed on the battery to obtain impedance and characteristics of battery in response. The input signal to carry out EIS measurement can be either voltage (potentiostatic mode) or current (galvanostatic mode) [24]. In the potentiostatic mode, the impedance of a systems is determined by applying fixed potential to the battery and measuring the resulting current. The current response to the applied sinusoidal potential is also sinusoidal signal at the same frequency but there is a phase shift between applied voltage and the current response as shown in the Figure 1.6. On the other hand, in the galvanostatic mode, EIS is performed at a fixed current. Impedance of a system is determined by measuring the resulting voltage.

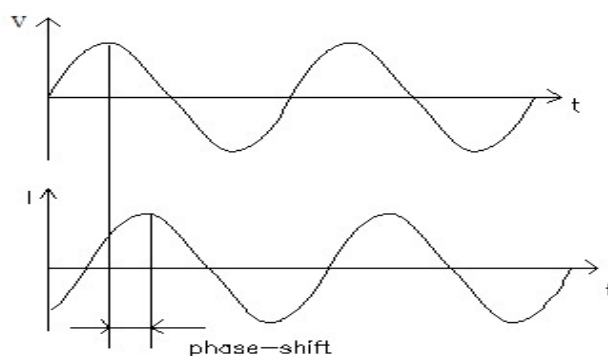


Figure 1.6 Sinusoidal current response to the applied potential and phase shift [28].

In potentiostatic control, the current response and the phase shift are recorded as responses of the measurements. By using the equation, impedance Z can be calculated:

$$\underline{Z} = \frac{u(t)}{i(t)} = \frac{\hat{U} \cdot \sin(\omega t)}{\hat{I} \cdot \sin(\omega t + \Phi)} = |\underline{Z}| \cdot \frac{\sin(\omega t)}{\sin(\omega t + \Phi)}, \quad (10)$$

where \hat{I} is the amplitude of the current signal, \hat{U} is the amplitude of the voltage signal, and Φ is the phase shift. The symbol of $|\underline{Z}|$ is the absolute value of the impedance [24]. The angular frequency is expressed as ω (expressed in radians/second) and is calculated from the following equation:

$$\omega = 2\pi f. \quad (11)$$

Impedance data can be described as a complex function and can be separated into a real part Equation 12, an imaginary part, $-Z''$ in Equation 13 and total impedance, $|\underline{Z}|$ is given by Equation 14 [24]

$$Z' = |\underline{Z}| \cdot \cos \Phi, \quad (12)$$

$$Z'' = |\underline{Z}| \cdot \sin \Phi, \text{ and} \quad (13)$$

$$|\underline{Z}| = \sqrt{Z''^2 + Z'^2}. \quad (14)$$

In EIS measurement nyquist plots are the most common plots. However, Nyquist plots often do not display any information about time and frequency of measured point. Most of the time, Bode points are included in the EIS measurements to identify the frequency at measured point. Generally, the Nyquist plot of fresh batteries (uncycled) is generally composed of one semicircle and one 45 degree linear diffusion line as shown in Figure 1.7.

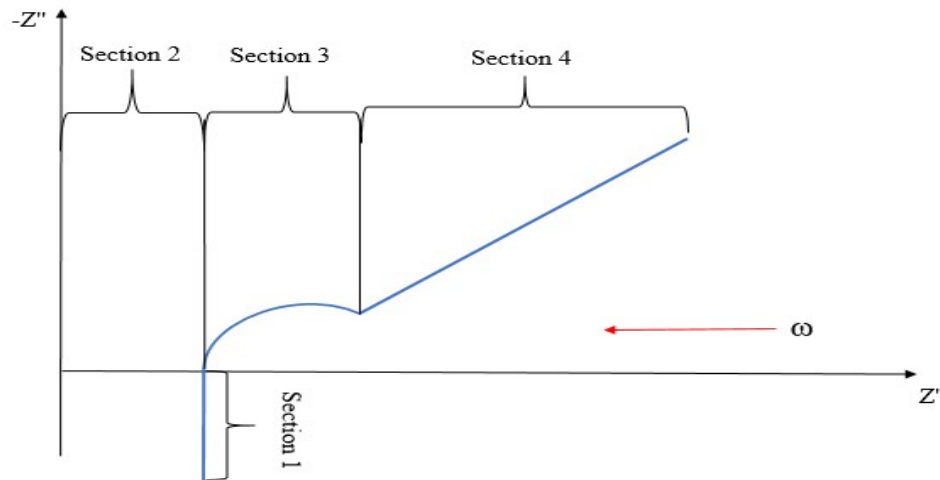


Figure 1.7 General Nyquist plot of fresh LIBs.

In the Nyquist plot of fresh conventional lithium ion batteries, the first section represents the inductive behavior of the wire in the battery. The second section indicates the sum of contact resistances of electrodes, electrolyte, separator and current collectors. The semicircle in Section 3 can be attributed to the electrolyte resistor and double-layer capacitor behavior in the Li-ion batteries. The last section of the Nyquist plot of fresh LIBs shows diffusion line at very low frequencies. The Nyquist plots of cycled Li-ion battery has two semicircles and ideally 45° linear diffusion line. It is generally accepted that for both EIS of fresh battery and EIS of cycled battery, spectrum at very high frequency regions (Section 1) displays inductive properties triggered by metallic components in the battery along with electrical cables. In Section 2, for the Nyquist plot of cycled batteries, the ohmic resistance of the battery from the origin to the intersection of the Nyquist plot with the real x axis is the sum of the resistances of components of battery which are current collectors, separator, electrodes and electrolyte [24].

The semicircle of Section 3 which is the high frequency semicircle is due to the phenomenon of SEI (Solid Electrolyte Interphase) region forming on the surface of anode during cycling process. The semicircle of Section 4 which is the middle frequency semicircle, represents the impedance of the charge transfer reaction and double layer capacity at electrodes. The low-frequency Warburg impedance is the diffusion process in the active material of the electrodes at as shown in section 5 [21, 24]. The representation of the Nyquist plot of a cycled LIB is shown in Figure 1.8.

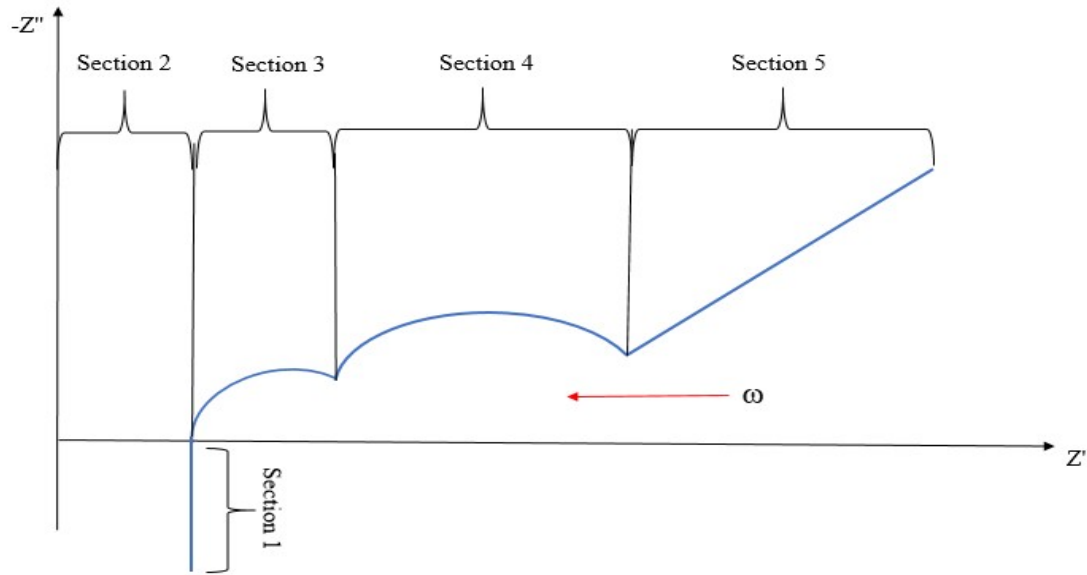


Figure 1.8 General Nyquist plot of cycled LIBs

The most common method of predicting the performance and interpreting the modeling data from the EIS measurements at different conditions and loads is the simulation based equivalent circuits (EC) [20, 22]. The real impedance data from measurement is firstly imported into optimization software and interpreted by an equivalent circuit model (ECM) which consists of resistances (R), inductances (L), capacitances (C), Warburg Impedances (W), and constant phase elements.

As a result of this interpretation, solid electrolyte interface (SEI) resistance, charge transfer resistance, and interphase electronic contact resistance that represent the electrical contact between current collectors and electrode components can be determined precisely. The elements of equivalent circuit models can be connected in parallel or in series to obtain complex equivalent circuits [31]. The change in physical and electrochemical properties of the battery can be evaluated with EC [21]. EIS is applicable on Li-ion batteries at every stage. However, identification of parameters and prediction of elements of EC must be well understood. The circuit element resistance, R which has no imaginary part has the impedance of

$$Z_R = R. \quad (15)$$

The impedance of capacitance does not have a real part. It has only an imaginary part. The impedance of capacitors is the function of frequency and is inversely proportional to the frequency [31]. The current of capacitor is phase shifted -90° with respect to applied voltage. Equation 16 shows the calculation of impedance of capacitors [31]

$$Z_C = \frac{1}{j\omega C}. \quad (16)$$

An ideal capacitor is based on the homogeneous electrochemical modeling. In the case of lack of homogeneity, constant phase element, Q is used as a circuit element. Equation 17 represents the impedance calculation of CPE [31]

$$Z_{CPE} = \frac{1}{Y_0(j\omega)^n}, \quad (17)$$

where, Y_0 is the admittance of an ideal capacitance and n is an depression factor, ranging from 0 to 1.

When $n = 1$, the CPE acts as a pure capacitor, while when $n = 0$, the CPE acts as a pure resistor. In addition, when $n = 0.5$, the CPE acts as a Warburg element. With Autolab analyzer, double layer capacitance and coating capacitance are generally modelled with a CPE [23, 31]. Ion diffusion in electrochemical systems are modeled with the Warburg impedance. The Warburg impedance can be calculated as shown in the Equation 18

$$Z_w = \frac{1}{Y_o \sqrt{j\omega}}. \quad (18)$$

A Warburg impedance has real and imaginary parts, resulting in phase angle of phase angle of 45° . Y_0 is the admittance of diffusion. Inductors have mainly imaginary parts like capacitors. The impedance of an inductor is proportional to the frequency and increases with the increasing frequency. The current of inductor is phase shifted 90° with respect to applied voltage. Equation 19 shows the calculation of impedance of capacitors [31]

$$Z_L = j\omega L. \quad (19)$$

Flexible lithium ion batteries used in EIS measurement, testing site, equivalent circuits and its components for fitting and simulation of data from IES measurement are discussed in detail in Chapter 2.

Chapter 2 Experiments

2.1 Overview

In this chapter, the materials incorporated in the flexible Li-ion batteries, the equipment used in the experiments, and the fabrication process including the preparation of the electrodes, current collectors and solid polymer electrolytes will be presented in detail. Subsequently, the capacity measurement techniques to investigate the functionality of the batteries will be provided. Finally, the buckling tests for each single battery using the tensile machine apparatus with *in situ* EIS measurements at different buckling curvatures will be discussed, and descriptions of the Nyquist plots of fresh and cycled flexible lithium ion batteries, model fitting techniques and simulation-based EIS equivalent circuits to determine battery characteristics will be discussed.

2.2 Materials

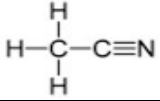
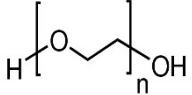
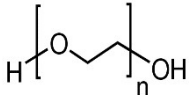
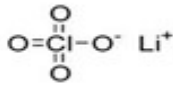
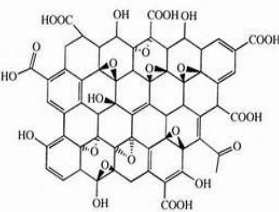
The specific properties and sources of the materials used in the fabrication of flexible lithium-ion batteries are presented in Tables 2.1 and 2.2. The current collectors and electrodes were purchased from MTI Corporation, and were then, cut to the intended dimensions to be used in the battery. In addition, copper tape was purchased and used as a current conductor. The properties of current collectors, electrodes and current conductor are listed in Table 2.1. The solid polymer electrolyte which transports the positive lithium ions and acts as a separator during the charge/discharge cycling process of the battery is prepared in the laboratory. Acetonitrile was purchased from Sigma Aldrich and used as a solvent. Two different PEO polymers with different molecular weights were used as polymer electrolyte, also purchased from Sigma Aldrich.

The lithium perchlorate (LiClO_4) is used as lithium salt and the graphene oxide (GO) as nanofiller is added to the solid polymer electrolyte to enhance its ionic conductivity. Table 2.2 shows the properties of the materials that are used for the preparation of the solid polymer electrolyte in the laboratory.

Table 2.1 Material properties of current collectors, electrodes and current conductors.

Name	Component	Material	Thickness	Specific capacity	Average cycle life	Source
Li-Ion Battery Cathode - Aluminum Foil Single Side Coated by LiCoO_2	Current collector	Aluminum	0.015mm $\pm 0.003\text{mm}$	N/A	N/A	MTI Corporation
	Cathode	Lithium Cobalt Oxide (LiCoO_2)	0.085mm $\pm 0.008\text{mm}$	145mAh/g	500 Cycles at 0.2C	
Li-Ion Battery Anode - Copper Foil Single Side Coated by Graphite	Current collector	Copper	0.01mm $\pm 0.005\text{mm}$	N/A	N/A	MTI Corporation
	Anode	Composite Graphite	0.04mm $\pm 0.008\text{mm}$	330mAh/g	N/A	
Copper tape	Current conductor	Copper	0.207 mm	N/A	N/A	N/A

Table 2.2 Materials used in the preparation of solid polymer electrolyte.

Name	Molecular Formula	Molecular Structure	Molecular Weight	Source
Acetonitrile	C_2H_3N		41.05	Sigma-Aldrich
Poly(ethylene oxide)	$H(OCH_2CH_2)_nOH$		100,000	Sigma-Aldrich
Poly(ethylene oxide)	$H(OCH_2CH_2)_nOH$		600,000	Sigma-Aldrich
Lithium Perchlorate	$LiClO_4$		106.4	Sigma-Aldrich
Graphene Oxide	N/A		N/A	Graphene Supermarket

2.3 Equipment

The equipment used in the experiments conducted for this study, are listed in Table 2.3. Figure 2.1 shows the vacuum dry glove box used to store the initial constituent materials, SPEs and flexible LIBs. Large and small chambers enables the transfer of objects of various sizes inside and outside of glove box. The membranes were dried in the vacuum ovens shown in Figure 2.2.

Table 2.3 Equipment used in the experiments.

Name	Type	Function	Source
Analytical Balance	PA 200 C	Weighing	Intell-Lab™
Magnetic Stirrer	RT 15 power	Mixing and Stirring	IKAMAG
Sonicator	3510	Ultrasonic Cleaning	Branson
Vacuum Oven	N/A	Dry	SHELAB
Glovebox Systems	Dual Port- Omni Lab	Battery Assembly and Dry Storage	Vacuum Atmospheres company
Lamination Machine	Saturn 95	Laminating	Fellowes
Tensile machine	MARK-10 ESM301L	Buckling Test	Cole Parmer
Autolab	N Series	Capacity Measurement	Metrohm
Autolab	N Series	EIS Measurement and Fitting	Metrohm
High Temperature Measurement Oven	N/A	50 °C Battery Testing	Espec
Autolab	N Series	50 °C EIS measurement	Metrohm



Figure 2.1 Glove box system.



Figure 2.2 Vacuum Oven.

2.4 Fabrication Process

Current collectors, electrodes, solid polymer electrolyte, current conductors and lamination sheets are needed for the fabrication of the flexible lithium ion battery. Current collectors, electrodes and current conductor are obtained from various manufacturers and cut to the desired dimensions. As mentioned previously, solid polymer electrolyte (SPE) is prepared in the laboratory. Basically, specific amount of PEO powder and lithium salt polymer are dissolved in the acetonitrile and then, the graphene oxide (GO) is added to the solution as a nanofiller. Because of its properties, graphene oxide has the potential to be applied in ultra-thin energy storage devices, flexible electronics, and sensor devices [19]. Solid PEO–LiClO₄–GO nanocomposite electrolyte with 1 wt% GO has been recently reported to show about two orders of magnitude enhancement in ion conductivity ($\sim 10^{-5} \text{ S cm}^{-1}$) compared to pure polymer electrolyte (PEO–LiClO₄) ($\sim 10^{-7} \text{ S cm}^{-1}$) [17]. Furthermore, the tensile strength of the nanocomposite electrolyte with GO has shown to increase by 260% compared to that of the pure polymer electrolyte. This increase in tensile strength can be attributed to the superior mechanical properties of GO nanosheets and playing the role of “tie molecule” in the polymer host. [17]. It has also been reported that the addition of GO can lead to lower internal and interfacial impedance demonstrated by EIS measurements [16]. After the preparation of the SPE, it is also cut to the desired dimensions. Finally, all prepared components are assembled into a battery. The fabrication process is explained in detail in this section.

2.4.1 Preparation of Solid PEO (100,000 Mw)/GO/LiClO₄ Electrolyte

The PEO powder (2g), the lithium perchlorate (0.3g) (ether-oxygen to lithium ratio (EO/Li) of 16 : 1) and graphene oxide (0.021g) which is 1 wt. % (percent of total weight of the polymer electrolyte film) are precisely weighed on the analytical balance and 70 mL acetonitrile (C₂H₃N) is set based on the measuring glass [16]. For better mixing, the preparation of solution must be done under stirring. Therefore, 60 mL acetonitrile was poured into a round glass jar. Subsequently, a magnetic stirring bar was placed inside the pure acetonitrile in the jar, and the jar was placed on the magnetic stirrer. While stirring the acetonitrile, first, the PEO powder was slowly added into the acetonitrile solvent. Thereafter, the Li salt and GO powder were added into the jar. They were all mixed in a round glass jar to dissolve the PEO powder and Li salt in acetonitrile. This procedure was applied to yield homogenous and mechanically stable membranes. The solution was stirred for 24 hours to obtain PEO/GO/Li salt solution. After stirring, the solution was sonicated for 30 minutes. Simultaneously, non-stick Teflon petri dish was cleaned and washed with acetone, and was placed into the oven at 50 °C for 15 minutes for drying. Then, PEO/GO/LiClO₄ solution was poured into cleaned and dried petri dish. Teflon petri dish was placed inside the vacuum oven at 50 °C and was kept there for 20 hours to produce a dry membrane. During the drying process, continuous vacuum was applied for a more effective drying of the membrane and to prevent exposure to the air. Finally, the SPE film was stored in the vacuum glove box for seven days to make it fully dry and prevent it from absorbing moisture and plasticization before use.

2.4.2 Preparation of Solid PEO (600,000 Mw)/GO/LiClO₄ Electrolyte

For the preparation of the second type of SPE with the PEO of a different molecular weight (i.e., 600,000 Mw), the same procedure was followed as for the first electrolyte. While stirring the acetonitrile solvent, the PEO powder (2 gr), the lithium perchlorate (0.3g) and 1 wt. % graphene oxide (0.021g) were added and dissolved in 70 mL acetonitrile in a jar on magnetic stirring machine. The solution was stirred for 48 hours. After stirring, the solution was sonicated for 60 minutes to break off the potentially aggregated particles. Petri dish was cleaned with acetone and was placed into the oven at 50 °C for 15 minutes of drying. Afterward, the solution was poured into the clean petri dish and the petri dish was placed inside the vacuum oven at 50 °C for 24 hours. This higher molecular weight (600,000) SPE does not absorb moisture or plasticize as quickly as the first electrolyte (100,000 Mw PEO) and therefore, it was stored in the vacuum glove box for three days before use.



Figure 2.3 Preparation of the solid nanocomposite electrolyte.

2.4.3 Preparation of Current Collectors and Electrodes

The cathode/current collector bilayer sheet used in the Li-ion battery is based on an aluminum foil coated by lithium- cobalt oxide in single side and was purchased from MTI Corporation. Anode/current collector sheet used in the Li-ion battery is based on the copper foil coated by graphite in single side and was also bought from MTI Corporation. All information about those sheets can be found in Table 2.1. Electrodes and current collectors from MTI Corporation are cut to size of $20 \times 20 \text{ mm}^2$ by using paper cutter. Then, the copper tape is cut to a length of 30mm sections and is then attached on both surfaces of the current collectors as a current conductor to enable connection to the equipment for battery charging and discharging and to measure the kinetics that occur inside the battery. The electrodes and current conductors are stored in the glove box until use.

2.4.4 Fabrication of Flexible Lithium-ion Battery

After the SPE, electrodes, current collectors and laminating sheets are ready to use, the battery assembly process was performed in the glove box where all the components of flexible lithium ion battery are stored. First, the copper current collector coated by graphite was placed on the laminating sheet. For ideal achievement of SPE properties including the ionic conductivity and interfacial contact, 5 to 7 wt % of plasticizer (aqueous 1 M LiPF₆ in ethylene carbonate and dimethyl carbonate (EC/DMC 1: 1 vol/vol)) were added on the surface of the graphite anode and on the surface of LiCoO₂ cathode [19]. Subsequently, the solid polymer electrolyte was sandwiched between the anode and cathode.

Figure 2.4 from a previous work by this research group [16] shows that such fabricated flexible lithium ion battery is functional and the battery lightens the red LED. In addition, the components for the fabrication of flexible battery can be seen in this figure. Additional images of the fabricated batteries will be provided in the next chapter.

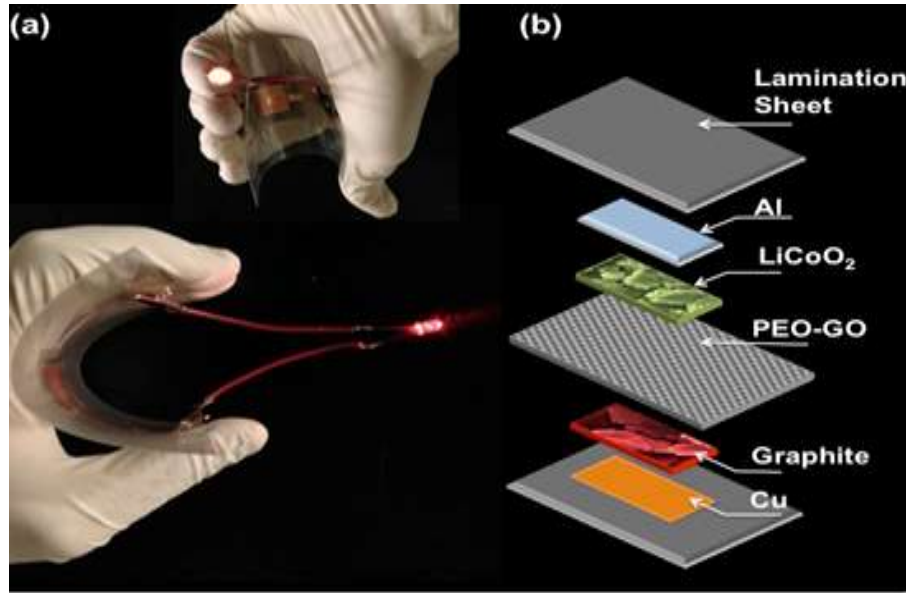


Figure 2.4 Fabricated flexible LIB powering an LED and layers of flexible LIB [16].

Table 2.4 Properties of components used in the fabrication of the battery.

Component	Material	Quantity	Length	Width	Thickness
Anode	Graphite	1	20 mm	20 mm	0.04 mm
Current Collector (Anode)	Copper (Cu)	1	20 mm	20 mm	0.01 mm
Cathode	LiCoO ₂	1	20 mm	20 mm	0.085 mm
Current Collector(Cathode)	Aluminum (Al)	1	20 mm	20 mm	0.015 mm
Electrolytes	PEO+LiClO ₄ +1%GO	1	20 mm	20 mm	0.450 mm
Current Conductor	Copper	2	30 mm	5 mm	0.207 mm
Encapsulant	Scotch laminating sheet	2	N/A	N/A	0.069 mm

Table 2.4 shows the dimensions and the quantity of the components used in the fabrication of flexible LIBs. For better sealing and to avoid delamination under bending and buckling, glue was added around the battery between the laminating sheets, and the battery was double laminated as shown in Figure 2.5.



Figure 2.5 Double lamination process of the battery.

2.5 Characterization

As mentioned in the previous sections, each flexible Li-Ion battery was stored in the argon-filled glove box following their fabrication. For characterization, LIBs were taken out of the glove box one by one and were tested. Fresh and cycled batteries with different properties and treatments were characterized under loading. The first step was to conduct EIS to determine the impedance of each single battery and gain some insight on the functionality of the battery upon cycling. The prediction of the functionality of the fresh batteries was facilitated by observing the Nyquist plots of the batteries in certain frequency range.

After identifying the proper “functional” batteries according to their first EIS test, then a comprehensive EIS measurement was applied to the fresh batteries at different curvatures and it was also applied to the cycled batteries at similar curvatures. In this section, the capacity measurements, the EIS measurement at various curvatures, and the buckling/bending analysis applied to flexible lithium ion battery are described.

2.5.1 Capacity Measurement

Generally, to optimize the capacity of the battery and according to the internal resistance of the battery, different C rates and currents are chosen [32]. However, in this study capacity measurements were performed to determine the functional batteries to test under the buckling. Usually, a high cell operating voltage is desirable in order to achieve a high capacity and, a cell operating voltage is related to the cathode voltage. Using high-capacity cathode materials and using electrolytes with large voltage window, a high cell operating voltage can be achieved. However, for the stability of conventional electrolytes and a long battery lifetime, cutoff voltage must be chosen to remain in the safe window [34]. For non-conventional electrolytes such as polymer electrolytes with wider voltage window, cut-off voltage can be increased to higher values (i.e., 4.9 V or higher) [16]. 4.2 V is the upper cut-off voltage for charging LiCoO_2 and it corresponds to a lower potential than the theoretical capacity of the cathode, around 145 mAh/g which is shown in table 2.1. The lower cut-off voltage of flexible Lithium ion battery, 2.8 V provide residual capacity of around 30 percent after discharge. For Lithium ion batteries, 4.2 V to 2.8 V potential range is one of the most effective working bandwidth. Charging and discharging battery in this range causes reduced voltage related undue stress and leads longer service life of battery [33, 35].

1mA		
Remarks	Chrono potentiometry ($\Delta t > 1$ ms)	...
End status Autolab		...
Signal sampler	Time, WE(1).Current, WE(1).Potential	...
Options	No Options	...
Instrument	MAC80097#3	
Instrument description	battery 56	
+ Autolab control		...
- Repeat n times	20	
Number of repetitions	20	
+ Set current	0.000E+00	
+ Set cell	On	...
+ Record signals (>1 ms) galva..	[60, 1]	—
+ Wait time (s)	5	
+ Set current	1.000E-03	
+ Record signals (>1 ms) galva..	[10800, 20]	—
+ Wait time (s)	10	
+ Set current	-1.000E-03	
+ Record signals (>1 ms) galva..	[36000, 20]	—
+ Set cell	Off	...
+ Wait time (s)	60	
<...>		
<...>		

Figure 2.6 Capacity measurement procedure.

2.5.1.1 Capacity Measurement at Room Temperature

All batteries were discharged (Li-ion insertion) and charged (Li-ion extraction) between 10 to 20 cycles with 1 mA cycling current at 25 °C room temperature to investigate the functionality of the batteries and to observe if the impedance of the batteries have the same trend for the batteries with slow or fast capacity fading. During the cycling process, high cutoff voltage was set up for 4.2 V and low cutoff voltage set up for 2.8 V. In addition, the resting time between the battery charge and discharge was 60 seconds.

Shortly after the capacity measurement at room temperature, the batteries were placed in the tensile machine at the same room temperature. Once the batteries were buckled, the EIS measurements were performed.

2.5.1.2 Capacity Measurement at High Temperature

Similar to the batteries cycled at room temperature, a set of batteries were placed in the oven at 50 °C and were discharged (Li-ion insertion) and charged (Li-ion extraction) between 10 to 20 cycles with the 1 mA cycling current. Capacity measurements were conducted at 50 °C. The batteries were then taken out of the oven and placed in the tensile machine. The buckling test was applied to the batteries and EIS measurements were conducted. The upper and lower cut-off voltages and resting time for the batteries cycled in the oven, were the same as that of the batteries cycled at room temperature.

2.5.2 Buckling/Bending Analysis

To determine the impedance and the contact resistance of the battery at different amount of buckling via EIS, the buckling tests were performed using the apparatus of Mark-10 tensile machine (Esm3011 Type). The battery was placed exactly at the mid-distance of two apparatus to produce maximum buckling at the center of the battery. During the test, the vertically placed battery was bent with horizontal displacements of 0 mm, 10 mm, 15 mm and 20 mm. For each displacement, EIS measurements were taken three times to be sure that the battery has a stable impedance at that curvature. To determine the radius of the curvature at the center of the battery, a circle fit method was applied to the photo pictures taken during the measurement. The distance between the two was known and measured during the experiments. Radius of the curvatures for each battery at different displacements were calculated separately.

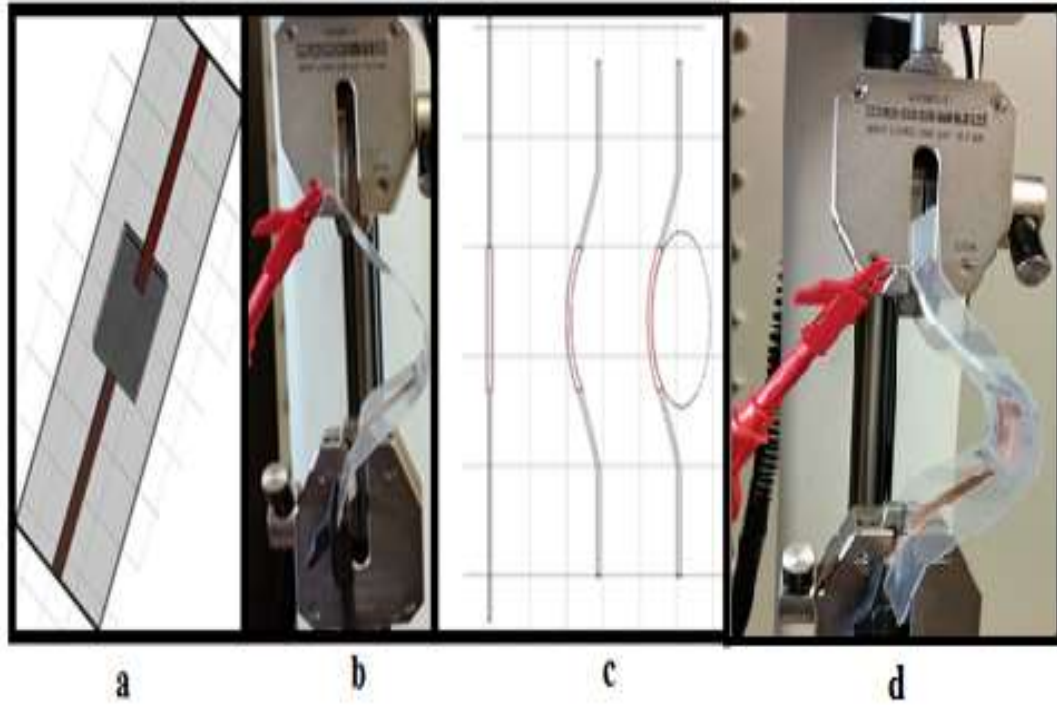


Figure 2.7 The buckling test and determining curvatures with circle fitting method.

Figure 2.7(a) represents the general structure of the fabricated battery. The current conductors were attached on two surfaces of the fabricated battery and the square-shaped battery was placed in the middle of the sealing with the laminating sheets. Figure 2.7(b) shows buckling of the flexible battery in the tensile machine. At the buckled position, EIS was performed by the addition of measurement electrodes. The circle fitting method to determine the buckling curvature is shown in Fig 2.7(c). In this figure that presents the side views of the battery, the red section at the center is the active battery area, and the transparent plastic section surrounding it, is the encapsulation laminating paper., The circle fitting was applied to the buckled battery at the center. Figure 2.7(d) shows the buckled battery at the center. All important factors that can affect the EIS measurement must be taken into consideration.

The buckling experiments were performed at the same speed so that all batteries could be treated in a same way. High speed buckling procedure must be avoided, because high speed buckling experiments can deteriorate the interface between the layers of the battery and can cause delamination of the layers and the laminating sheets. The tensile machine apparatus must be stationary and, furthermore, to ensure stabilized tensile grips, the EIS measurement was performed after 10 seconds of stabilization.

2.5.3 Electrochemical Impedance Spectroscopy

Electrochemical impedance spectroscopy (EIS) is a powerful method to characterize a battery or its components, and it is generally aimed at obtaining better insight and comprehension of the mechanisms in the battery including capacity fading. In this work, EIS measurement was conducted to investigate the change of contact resistance of different flexible lithium ion batteries subjected to increasing contact pressure. When the multi-layer battery is bent or buckled, the contact pressure between each layer increases. This increase in contact pressure can provide better interface contact between the layers of the battery which can potentially affect the contact resistance and the battery performance. The EIS measurement was divided into two categories: fresh batteries and cycled batteries. During the investigation of the flexible lithium ion batteries, the impedance spectra was recorded at flat position and at three different curvatures for both fresh and cycled batteries as mentioned in the previous section on buckling/bending analysis. All the impedance data were measured at room temperature (i.e., 25 °C) for both fresh and cycled batteries. Also, the batteries cycled at 50 °C in the oven were tested immediately after they were fully discharged at 25 °C.

The impedance measurement was repeated several times to obtain stable impedance spectrum and high statistical confidence. The experiments were carried out in the potentiostatic mode by applying fixed potential to the battery. The EIS was performed in a frequency range of 1 Hz to 0.1 MHz with amplitude of 0.01V using Autolab N-series analyzer as shown in Figure 2.8 with a frequency response analyzer (FRA) capability. The FRA has both potentiostatic and galvanostatic modes. In this experiment, the number of frequencies was set up to 50 producing plots with 50 impedance points each at a different frequency.

Frequency range

First applied frequency: 100000 Hz
 Last applied frequency: 1 Hz
 Number of frequencies: 50
 Significant digits: 5

Integration time calculation

Integration time (maximum): 0.125 s
 Integration cycles (minimum): 1

Amplitude

Amplitude: 0.01
☐ RMS

Frequency step

☐ Linear
☒ Logarithmic
☐ Square root
☐ Frequencies per decade

Wave type

☒ Single sine
☐ 5 sines
☐ 15 sines

Buttons: Replace, Add, Clear

	Frequency (Hz)	Amplitude (V)	Wave type	Integration time	Minimum number of cycles to integrate
1	100000	0.01	Single sine	0.125	1
2	79060	0.01	Single sine	0.125	1
3	62506	0.01	Single sine	0.125	1
4	49417	0.01	Single sine	0.125	1
5	39069	0.01	Single sine	0.125	1
6	30888	0.01	Single sine	0.125	1
7	24421	0.01	Single sine	0.125	1

Buttons: OK, Cancel

Figure 2.8 The frequency scan parameters.

The Nyquist plots present real and imaginary impedance parts of the measurement so that EIS measurements could be analyzed and interpreted quickly. The shape of the Nyquist plots plays an important role in the interpretation of the battery characteristics. The only disadvantage of the nyquist plots is that they do not show the frequency data. An alternative plot in the Autolab analyzer is the bode plot which can be used to observe the change of impedance and phase shifts as a function of frequency.

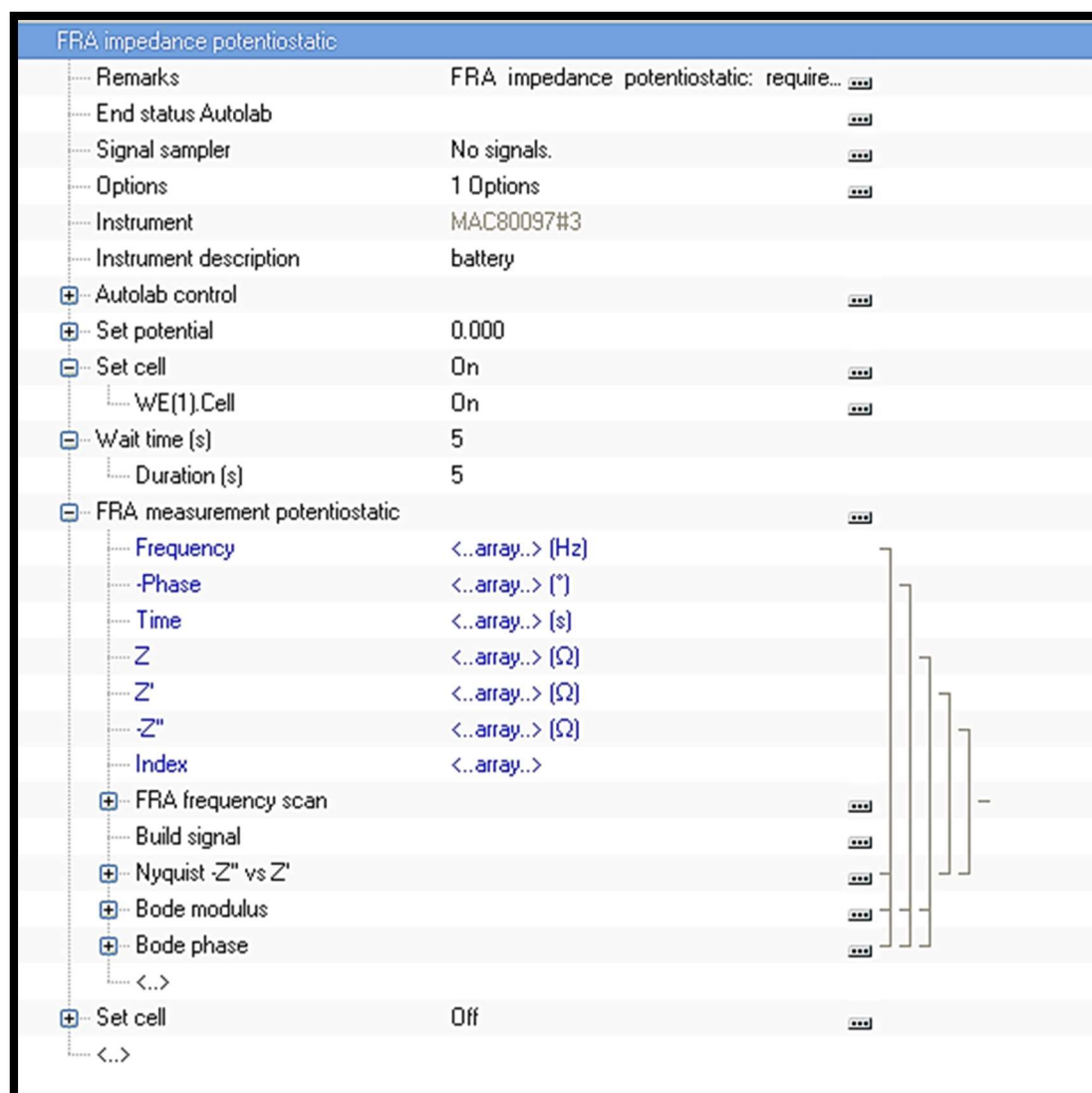


Figure 2.9 FRA potentiostatic procedure.

Curve fitting and simulation using equivalent circuits (ECs) were performed after impedance spectroscopy, to model the various transport and impedance mechanisms in the lithium-ion batteries. First, the parameters in the equivalent circuit model must be assigned according to the general working principle of the battery. Then, by means of the ECs, the Nyquist plots of the measured real impedance data were fitted via Autolab analyzer where the EIS measurements were performed.

2.5.3.1 Nyquist Plots and Circuit Modeling

The curve fitting of the real impedance data was used to identify the equivalent circuit (EC) elements and to obtain values for the solid electrolyte interphase (SEI) resistance. The SEI resistance in the fabricated flexible Li ion batteries in this work is expected to be negligible or relatively small due to the fact that the main electrolyte used is solid polymer, and only few drops of liquid electrolyte was used during the assembly to enhance the interface in the battery. EC elements must also include charge transfer resistance and the electrical contact resistance between the current collectors, electrodes and the polymer electrolyte. In this experiment, equivalent circuit models which were a combination of well-known circuit elements such as resistors(R), capacitors (C), constant phase element (Q) and Warburg impedance element (W) were effectively used to interpret the data from the impedance spectroscopy for the characterization of the electrochemical systems. While the impedance of the resistor has only a real part, the impedance of the capacitors which is a function of frequency, has only an imaginary part. Constant phase element and Warburg element have both real and imaginary parts. Figure 2.10 shows the equivalent circuit and the nyquist plot of the fresh batteries and Figure 2.11 shows the nyquist plot of cycled batteries.

Both Nyquist plots in the figures are ideal Nyquist plots. Because of the value of the contact resistance, the length and width of the first and the second semicircles and the angle of the linear diffusion line varies from battery to battery. In the equivalent circuit of the fresh battery, the first resistance R_C represents the first section of the Nyquist plot which gives the contact resistance value of the battery. In Section 2 of the Nyquist plot, the first semi-circle which is modeled by CPE and R elements in parallel connection gives the combination of the electrolyte resistance and the capacitance on the imaginary axis. Since there is no charge transfer for uncycled batteries, there is no charge transfer resistance. Therefore, there is only one semi-circle in this Nyquist plot, and it is only due to the polymer electrolyte resistance. When it comes to the capacitance, it is known that the SEI film forms after the initial charging. However, double layer capacitance can take place in fresh batteries and the capacitance effect observed in the Nyquist plot, can be attributed to the double layer capacitance in the fresh battery. In the last section of the Nyquist plot, the linear diffusion line is the Warburg impedance.

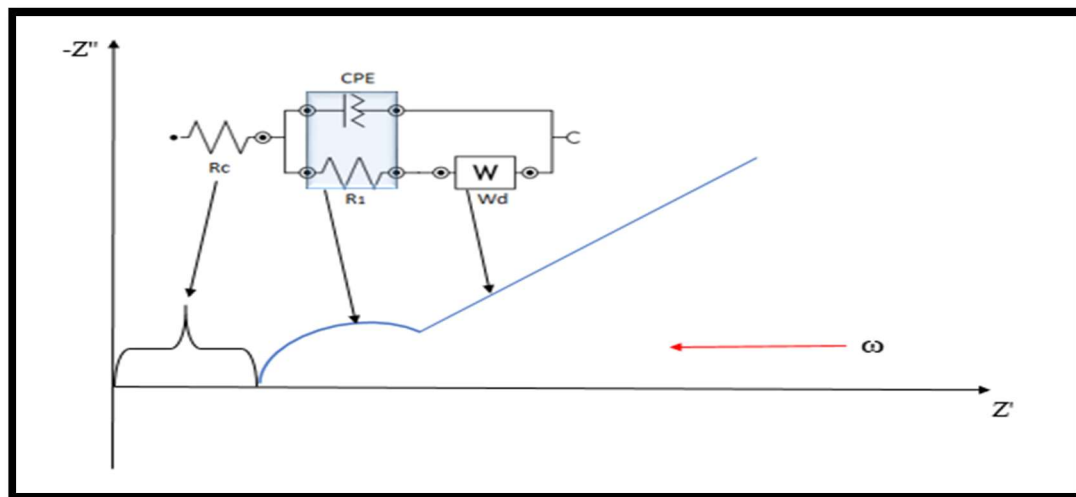


Figure 2.10 The equivalent circuit used for fitting of the Nyquist plot of a fresh battery.

The impedance of the fresh battery can be described as the sum of the impedance of the elements in the equivalent circuit. It is given by

$$\underline{Z} = R_c + \frac{1}{\frac{1}{R_1 + \frac{1}{Y_{0Q}\sqrt{j\omega}}} + Y_{0w}(j\omega)^n}. \quad (20)$$

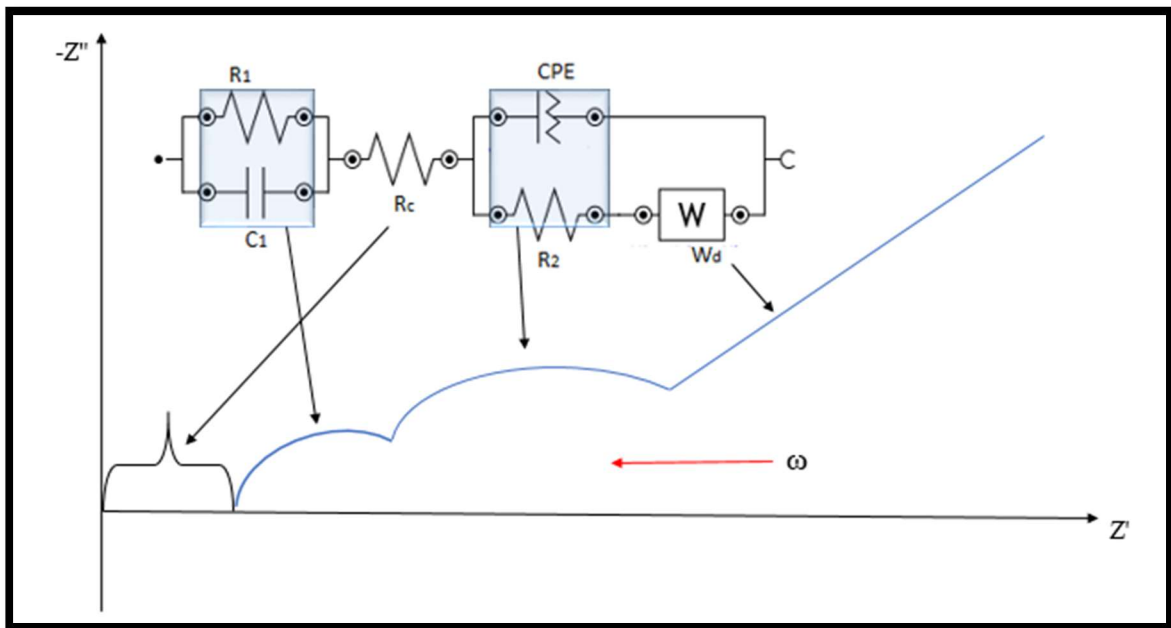


Figure 2.11 The equivalent circuit used for fitting of nyquist plot of cycled battery.

For the cycled batteries, the first section that is from the plot origin (0, 0) to the intersection of Nyquist plot with the real x-axis represents the contact resistance between the components of the battery. In the second section modeled by RC elements, the semi-circle consists of the resistance and capacitance. Resistance is mostly contributed by the electrolyte and potentially by a small amount of resistance arising from the SEI film formation. Capacitance of the first semi-circle can be originated from the SEI film formation and double-layer effect in the battery.

The second circle represents the combination of charge transfer resistance and the capacitance of double layers. Last section which is a linear diffusion line in the Nyquist plot is the Warburg impedance. The impedance of the cycled battery can be described as the sum of the impedance of the elements in the equivalent circuit. It is given by

$$\underline{Z} = \frac{1}{\frac{1}{\underline{Z}_{R_1}} + \frac{1}{\underline{Z}_C}} + \underline{Z}_{R_C} + \frac{1}{\frac{1}{\underline{Z}_{R_2} + \underline{Z}_W} + \frac{1}{\underline{Z}_{CPE}}}. \quad (21)$$

Insertion of impedances of each element leads to Eq. (22),

$$\underline{Z} = \frac{1}{\frac{1}{R_1} + j\omega C} + R_C + \frac{1}{\left(R1 + \frac{1}{Y_{0Q}\sqrt{j\omega}} \right) + Y_{0w}(j\omega)^n}. \quad (22)$$

After obtaining nyquist plots of fresh and cycled batteries and fitting them, values for circuit's elements were found and changes in contact resistances and contact conductance of batteries were investigated with respect to buckling curvatures. All Nyquist plots and the circuit models used to describe the changes in the contact resistances are presented in Chapter 3.

Chapter 3 Results and Discussions

3.1 Fabricated Flexible Lithium-ion Batteries

In this section, the results of the flexible battery fabrication process are presented and discussed. There are several aspects about the fabrication process that can lead to problems in the produced battery if not adequately addressed, and in general, the fabrication process must be performed very carefully. For example, the layers in the battery must be exact match of each other when it comes to dimensions of layers. Interface contact between the components of the battery plays a significant role in the battery performance. Under deformation, the deterioration in interface contact between the layers of battery can result in increasing resistance and performance loss. The delamination of laminated sheets under deformation may trigger the exposure of battery components to moisture and air. The reaction of the battery components with air and moisture can lead to the oxidation of components that can cause capacity degradation and failure and can render the battery functionless in the long term. Short circuit in flexible batteries is one of the most common problems that can cause nonworking batteries. Sliding of the layers on the top of each other, use of damaged or defected components, excessive addition of liquid electrolyte, and overheating of the battery in the laminating machine can cause problems in the final fabricated battery and must be avoided. Nanocomposite solid polymer electrolyte in Figure 3.4 is one of the most important components that can influence the impedance and performance of the battery. Over drying of solid polymer electrolyte in the oven generally causes porous surfaces of the electrolyte that may adversely affect the quality of the polymer electrolyte.

Also, overheating of the battery during the laminating process will damage the electrolyte. Both situations will lead to non-working batteries or batteries with very short service lives.

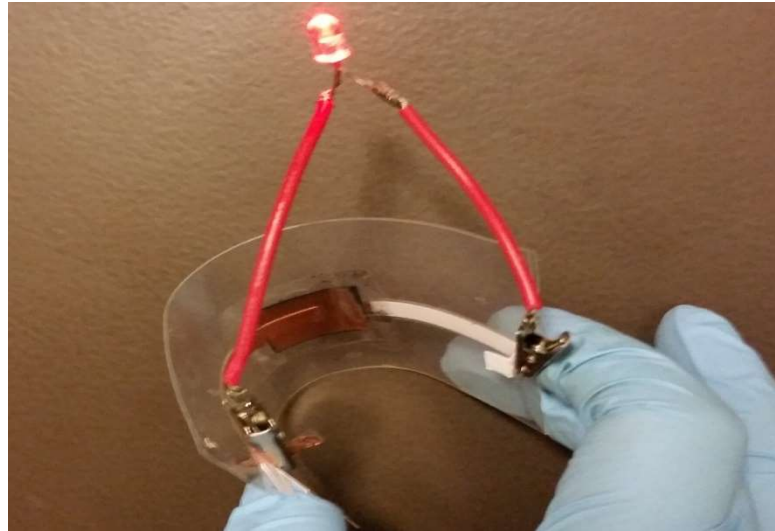


Figure 3.1 Fabricated flexible LIB powering the red LED.

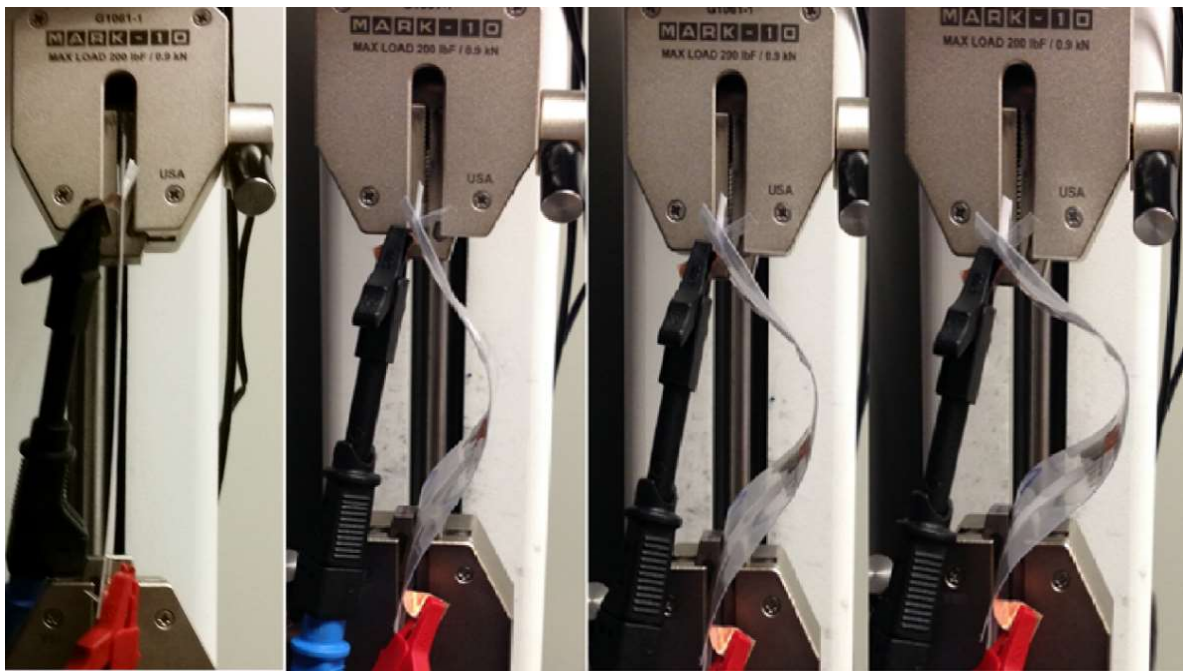


Figure 3.2 Flexible batteries at flat position and at three different curvatures.

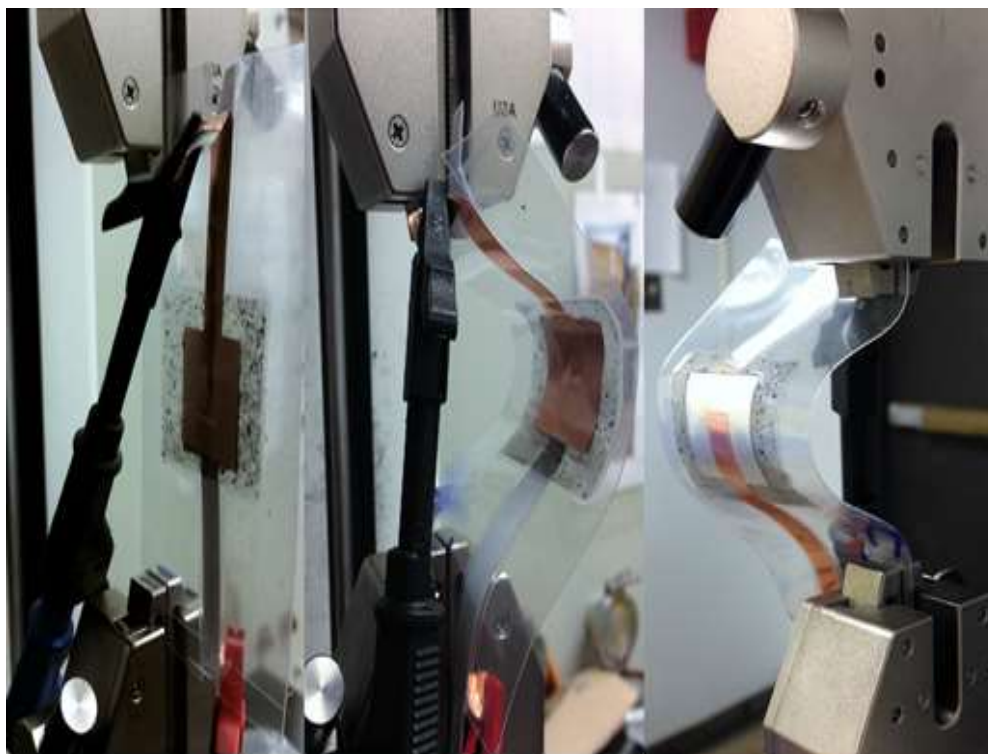


Figure 3.3 The fabricated battery at different curvatures and angles.

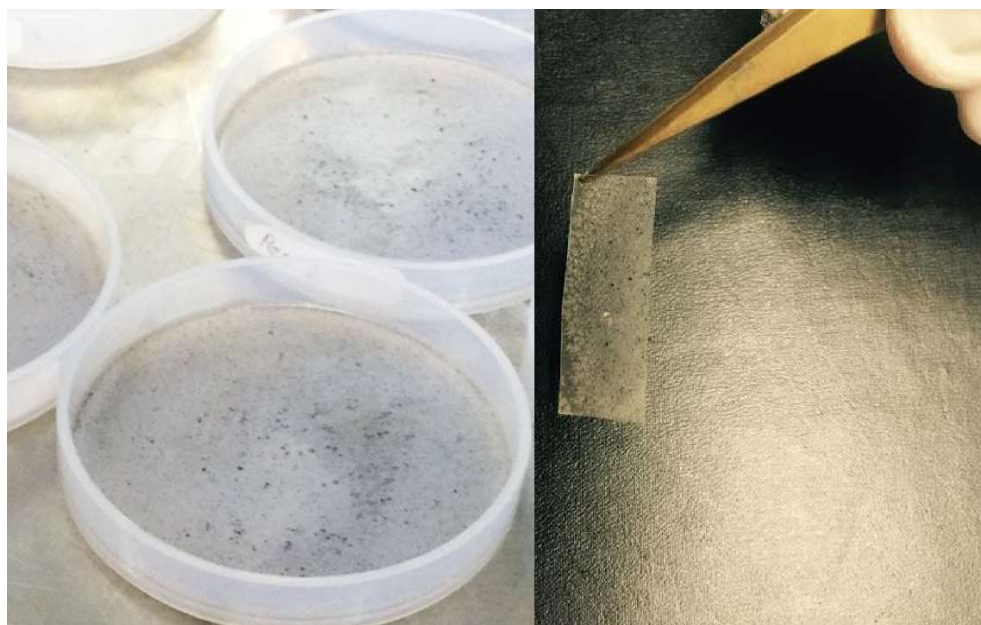


Figure 3.4 The nanocomposite solid polymer electrolyte.

3.2 Electrochemical Characterization of Flexible LIBs

Figure 3.5 presents the specific capacities of the first three batteries for 20 cycles at room temperature. Values of specific capacities of these cycled batteries start between 0.03mAh/cm^2 and 0.04mAh/cm^2 , and increases up to 0.065mAh/cm^2 and 0.08mAh/cm^2 .

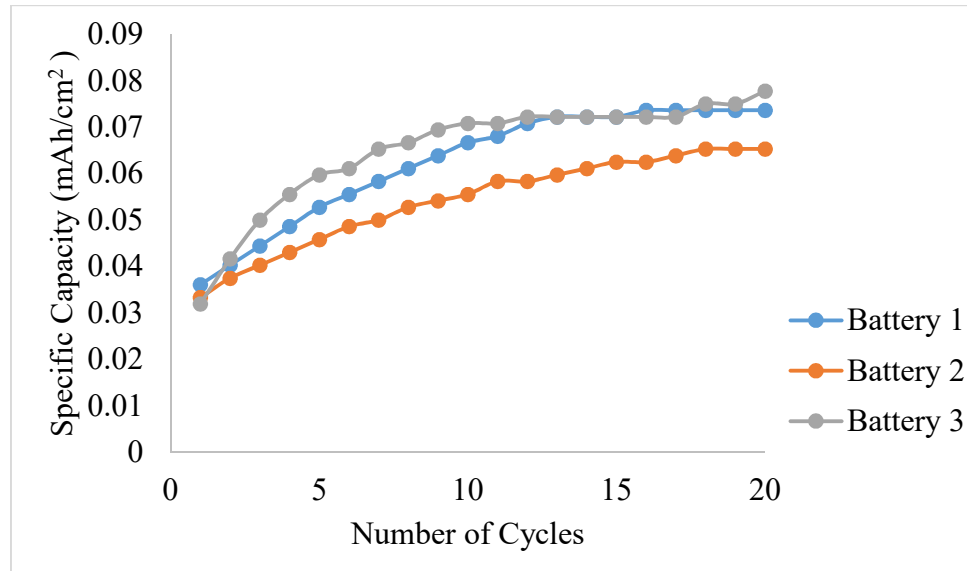


Figure 3.5 Specific capacities of Battery 1, Battery 2 and Battery 3 based on 100,000 Mw PEO at room temperature.

Figure 3.6 displays specific capacities of cycled batteries based on SPEs prepared with 600,000 Mw PEO host. Only these three batteries (Batteries 4-6) include the 600,000 Mw PEO. Other batteries are based on SPEs prepared with 100,000 Mw PEO. Batteries in this figure show various behaviors at different numbers of cycles. In Figure 3.6, specific capacities of Battery 4 and Battery 6 decrease gradually beginning from the first cycle. However, the specific capacity of Battery 5 increases from 0.052mAh/cm^2 to 0.075mAh/cm^2 .

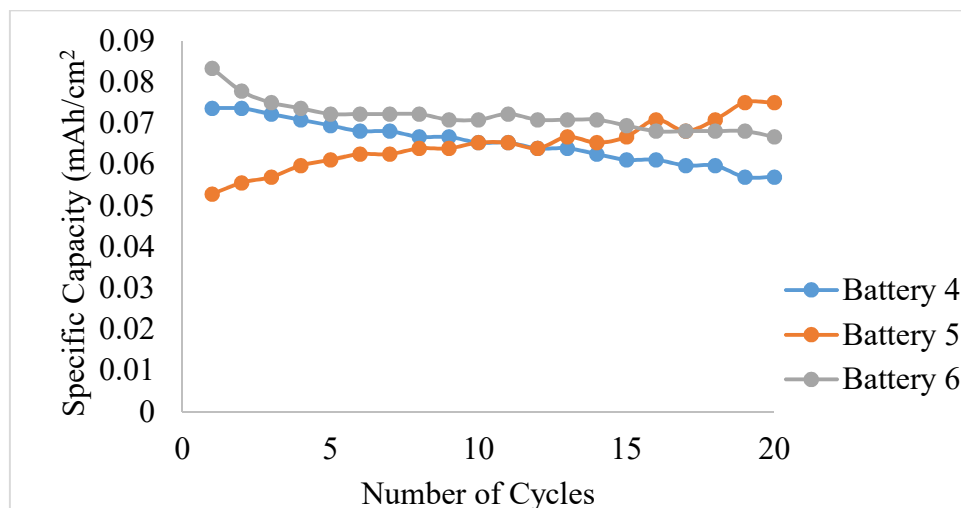


Figure 3.6 Specific capacities of Battery 4, Battery 5 and Battery 6 based on 600,000 Mw PEO at room temperature.

In Figure 3.7, after a small capacity fading, Battery 8 appears stable. Battery 9 had a large capacity fading between 0.15 mAh/cm² and 0.08 mAh/cm². On the other hand, the specific capacity of Battery 7 increases from 0.03mAh/cm² to 0.078 mAh/cm² as a result of 20 cycles. In comparison with the other cycled batteries, batteries cycled in the oven at higher temperature (i.e., 50 °C) have higher specific capacities.

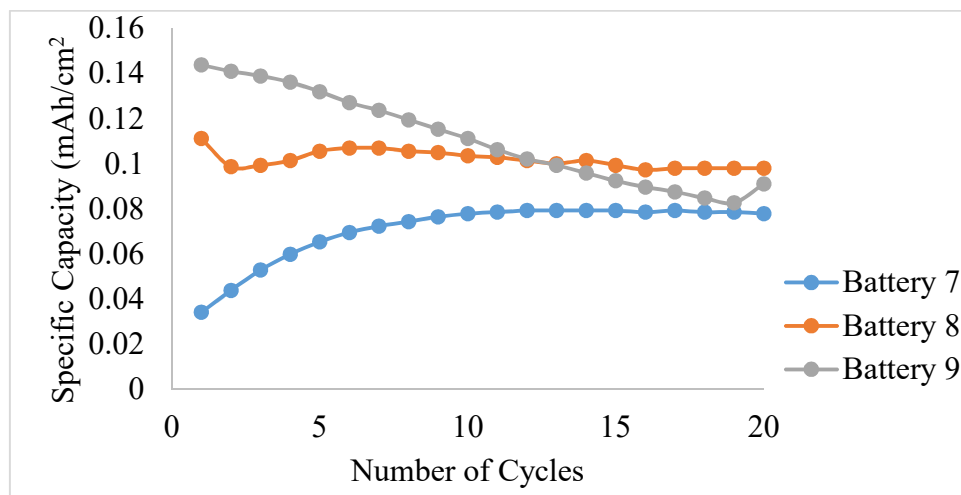


Figure 3.7 Specific capacities of Battery 7, Battery 8 and Battery 9 based on 100,000 Mw PEO at 50 °C.

3.3 Nyquist Plots of Fresh and Cycled Lithium Ion Batteries

EIS measurements were performed at four different curvatures for all batteries including flat position (zero curvature). Real data and fitting data obtained from fit-and-simulation based EIS on the Autolab analyzer are provided with Nyquist plots.

3.3.1 Nyquist Plots of Fresh Batteries

Nyquist plots of all fresh batteries, fabricated using SPEs prepared with 100,000 Mw PEO host, are presented and discussed in this section.

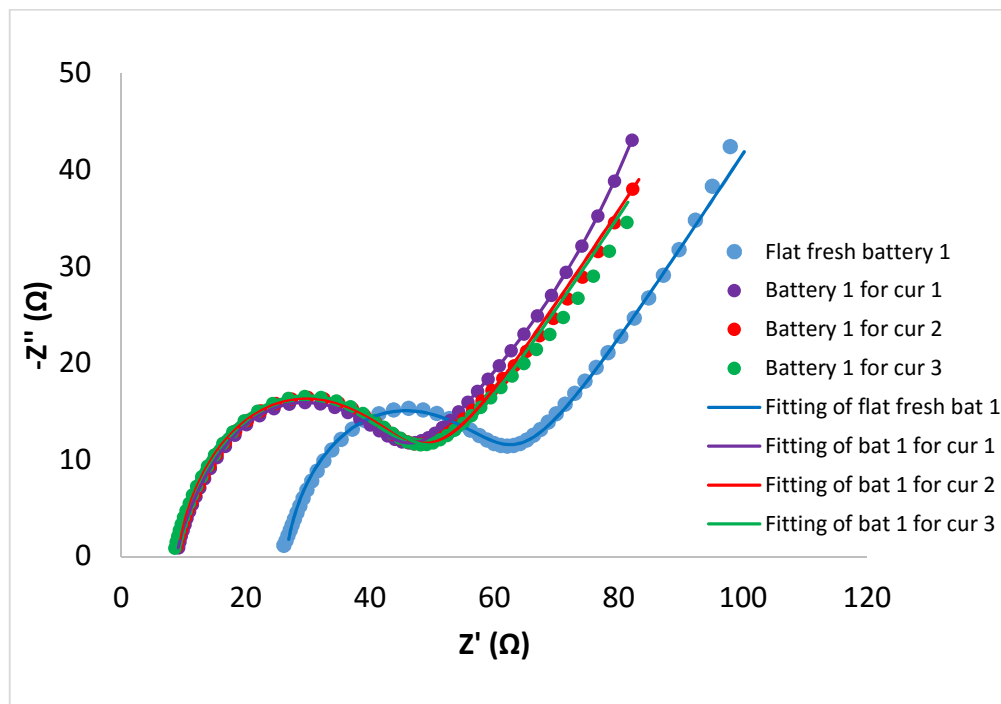


Figure 3.8 Nyquist plots of fresh Battery 1 at different curvatures.

In Figure 3.8, it can be clearly seen that the first section—between the origin and the intersection of the Nyquist plots with the real x-axis, which describes contact resistance between the components of the battery—decreases sharply under buckling compared to that in the flat position.

Even though the nyquist plots of Battery 1 for Curvatures 1, 2, and 3 seem to be similar, the green-colored plot that represents the highest amount of buckling has the lowest contact resistance. The general trend for the fresh Battery 1 is that with the increasing value of curvature, contact resistance decreases. Capacitances and linear diffusion lines are not affected significantly for Battery 1. The resistance of the first semicircle slightly increases under buckling, however the buckled battery has a clear advantage over the flat battery in terms of total resistance.

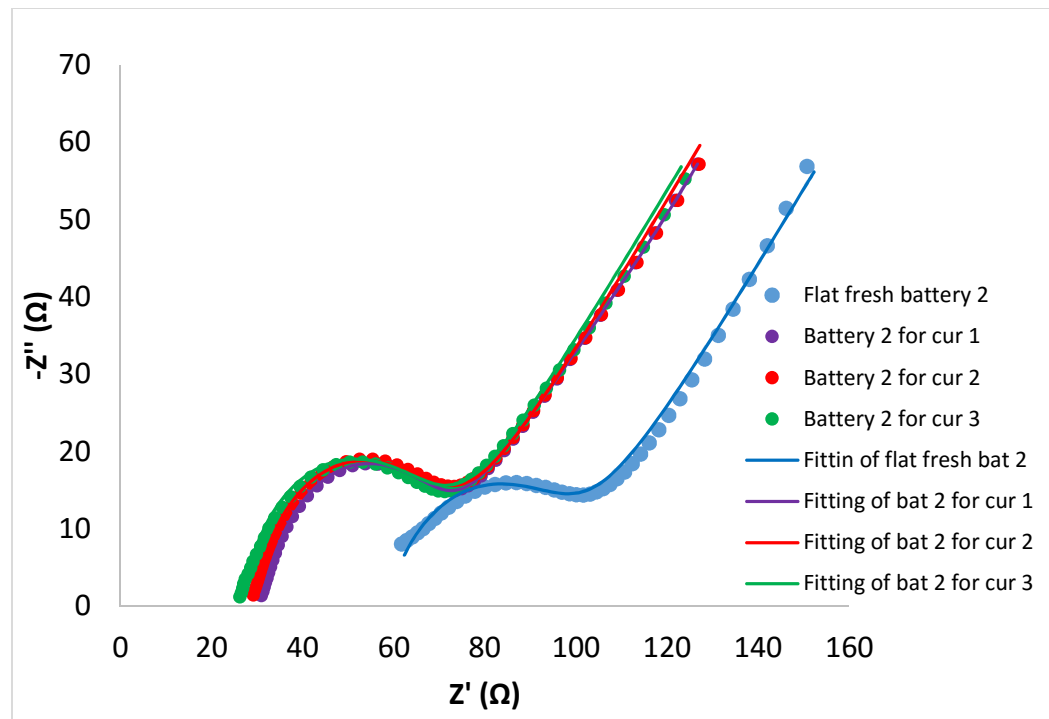


Figure 3.9 Nyquist plots of fresh battery 2 at different curvatures.

Similar to the fresh Battery 1, after the first buckling curvature, the contact resistance of Battery 2 shows a rapid decline compared to that at flat position as depicted in Figure 3.9. The green-colored plot has the lowest contact resistance, similar to the first figure.

By observing the width of the semicircle of Nyquist plots on the real x-axis, it is obvious that the battery at flat position has the highest resistance. From Curvature 1 to Curvature 3, the resistance of the semicircle changes insignificantly. The diffusion coefficient and the imaginary part of the semicircle on the y-axis, which represents the capacitance, do not show considerable changes.

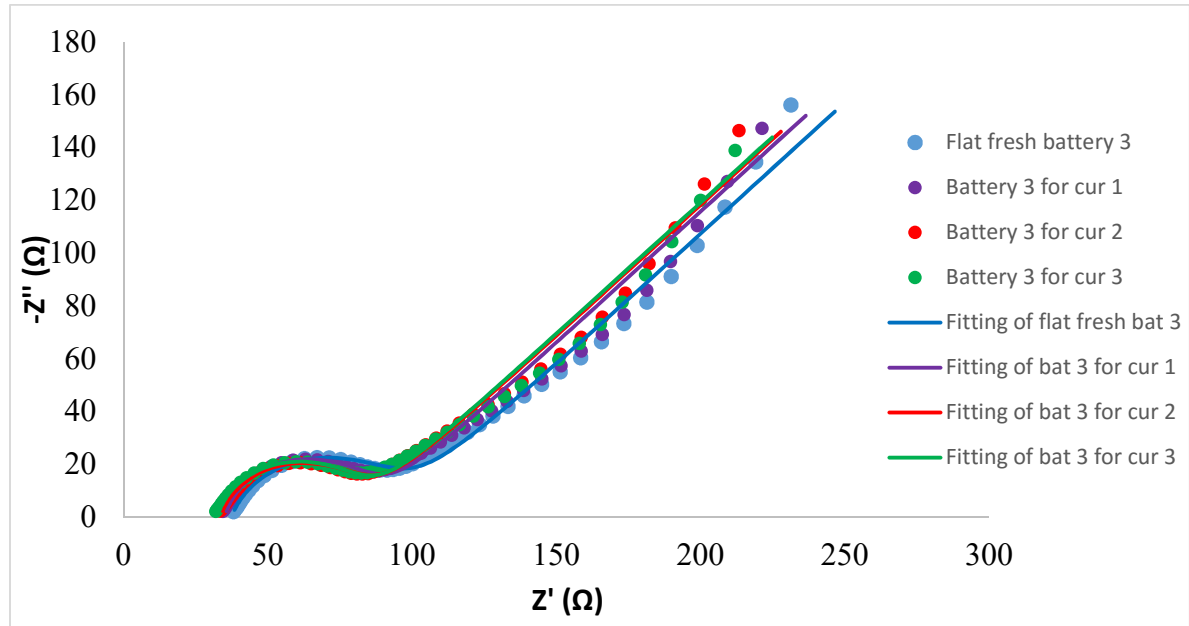


Figure 3.10 Nyquist plots of fresh Battery 3 at different curvatures.

Unlike the first two figures, all Nyquist plots for fresh Battery 3 for different curvatures seem to have approximate values in the Figure 3.10. Because of the longer linear diffusion line, the scale of the real x-axis in this figure is much larger than the scales of the x-axis of the first two figures. That makes the approximate values of resistances look like they are at the same point. In addition, from the flat position to the first buckling curvature, the first two fresh batteries have higher decline in the value of contact resistances. In Figure 3.10, the contact resistance for Battery 3 in the flat position is about 40 Ω , and the value of the contact resistance of Battery 3 at Curvature 3 is close to 30 Ω .

With the increasing radius of the curvature, this battery also exhibits the same trend that is decreasing of the contact resistance; but this decrease in contact resistance is comparatively less than the other two reduction values observed for Batteries 1 and 2. The value of resistance obtained from the semicircle in this figure also decreases slowly with the increasing radius of curvature. Buckling does not have a crucial effect on the capacitance value and diffusion, as in the first two batteries. Differences in the contact resistances of the fresh batteries can be attributed to the interfaces of the components in the batteries. For the first two fresh batteries, contact resistances sharply declined from the flat positions to the first buckling curvatures, and after the first buckling curvature, this decline became gradual. It can be observed that Battery 3 has a better interface compared to Batteries 1 and 2 initially. As they all buckled, the interfaces in the batteries comparatively improved (i.e., impedance decreased), although in the case of Battery 3 the improvement under buckling is observed to be relatively less.

3.3.2 Nyquist Plots of Cycled Batteries

The Nyquist plot of the next three cycled batteries, fabricated using SPEs prepared with 100,000 Mw PEO host, are presented and discussed in this section. Figure 3.11 shows the Nyquist plot of the first cycled battery. By carefully examining the figure, one may see that the Nyquist plots of Battery 1 after 20 cycles are composed of two semicircles. The first semicircle is in the high frequency (HF) region, the second depressed semicircle is in the middle frequency region, and a sloped line comprises the low frequency region.

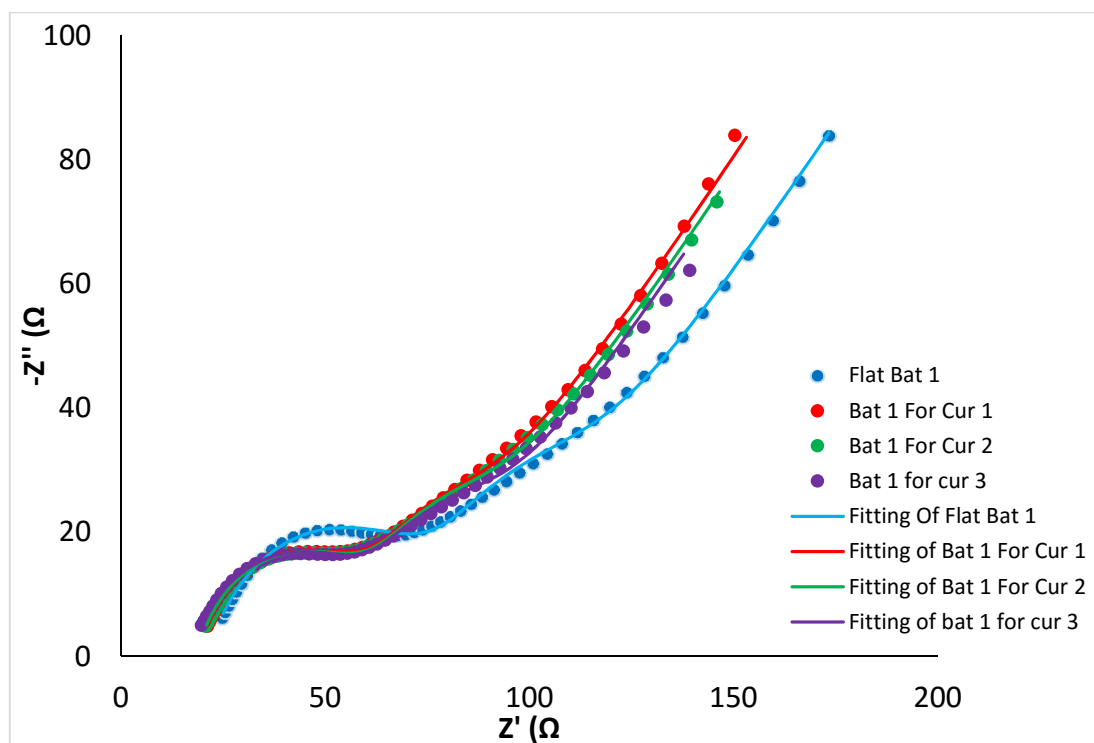


Figure 3.11 Nyquist plots of cycled Battery 1, fabricated using an electrolyte prepared with 100,000Mw PEO host.

By examining all the Nyquist plots, charge transfer resistance and contact resistance of Battery 1 show clear decline under the first buckling curvature in comparison to that in flat position. A slight drop in the contact resistance with increased buckling can be noticed by enlarging the figure. On the other hand, the capacitances of the first and second semicircles demonstrate negligible changes for different curvatures. Figure 3.12 shows the Nyquist plot of cycled Battery 2. The Nyquist plots of cycled Battery 2 after 20 cycles are composed of a linear diffusion line and two semicircles, similar to that in the first cycled battery.

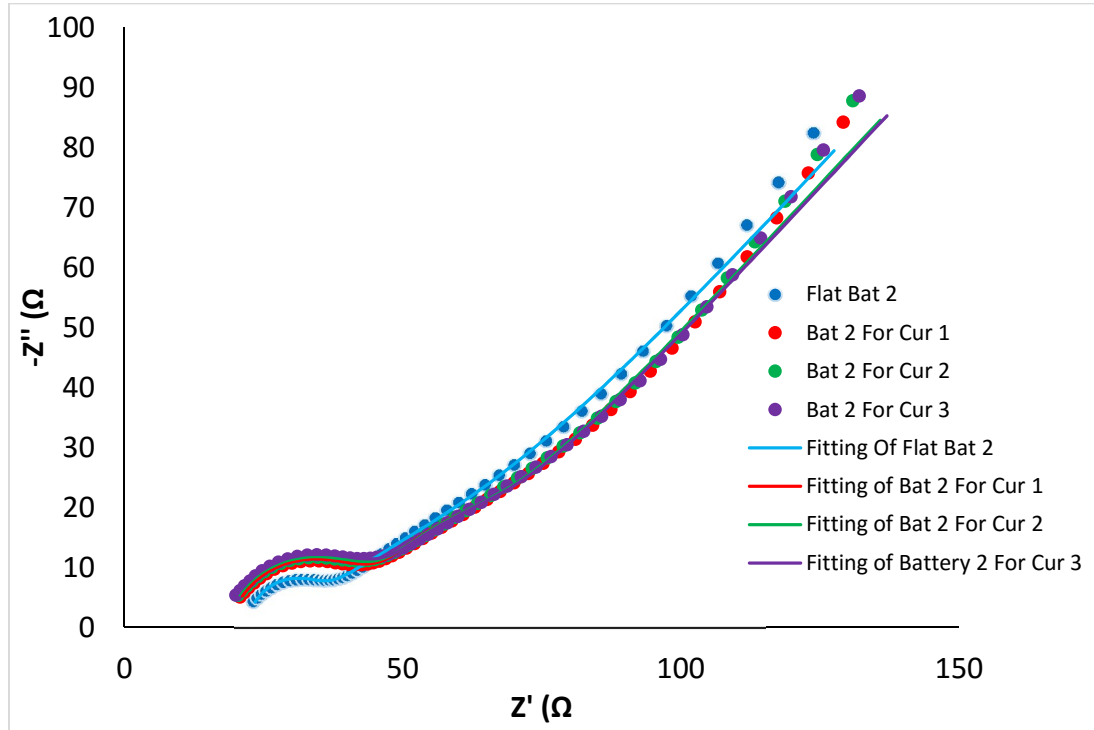


Figure 3.12 Nyquist plots of cycled Battery 2, fabricated using an electrolyte prepared with 100,000Mw PEO host.

The second semicircle can only be clearly observed by scaling up the mid-frequency region. The contact resistance and the charge transfer resistance both reduce with increased buckling, and furthermore, buckling leads to reduced total impedance for the cycled Battery 2. There were no significant changes in the capacitance due to the potential formation of SEI film or other passivation films, double layer capacitance or a Warburg impedance. In Figure 3.13, the Nyquist plots of the flat battery and buckled batteries seem to overlap, and all the Nyquist plots consist of two semicircles similar to that in the first two cycled batteries. The high frequency (HF) region semicircle shape is comparably obvious, whereas the second mid-frequency semicircle is highly depressed and less apparent.

The second semicircle has a much higher radius than the first one, and the only way to observe this circle is to magnify the figure between the first semicircle and the linear diffusion line. The values of the contact resistance and total resistance of the cycled Battery 3 demonstrate consistent reduction in impedance with increased buckling as in the case of the first two batteries.

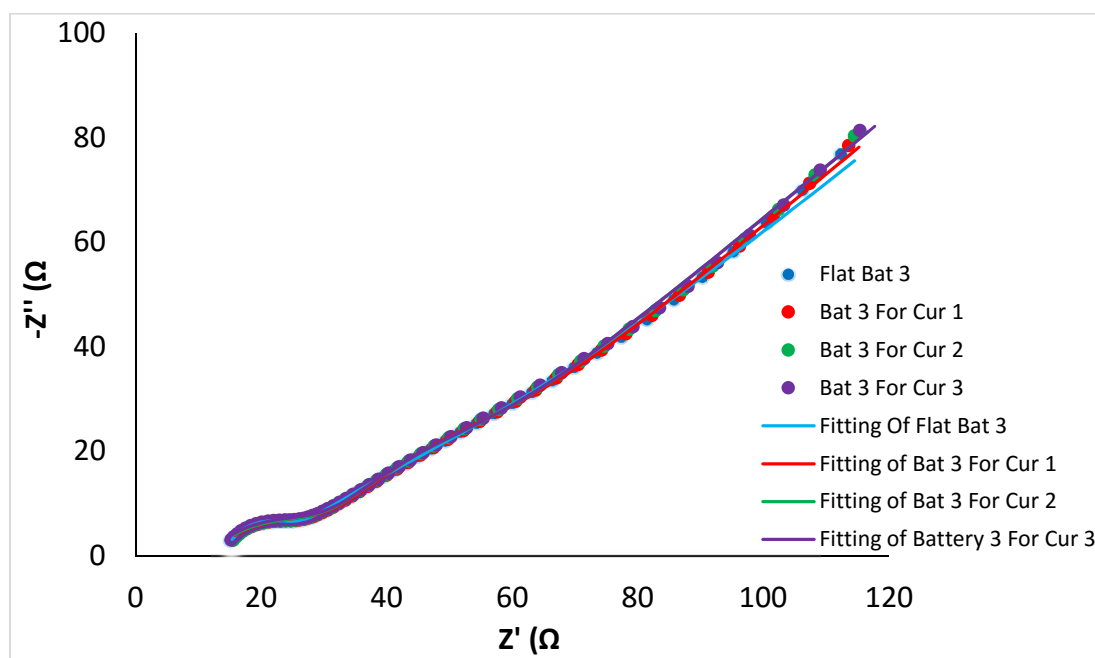


Figure 3.13 Nyquist plots of cycled battery 3, fabricated using an electrolyte prepared with 100,000Mw PEO host.

3.3.3 Nyquist Plots of Other Cycled Batteries

In this section, the Nyquist plot of the next three cycled batteries, fabricated using SPEs prepared with 600,000 Mw PEO host, are presented and discussed, and the Nyquist plots for the batteries based on 100,000 Mw PEO subjected to a higher temperature of 50 °C are also included.

Figure 3.14 shows the Nyquist plot of the cycled Battery 4 based on 600,000 Mw PEO tested at room temperature. The first cycled battery is composed of two depressed semicircles.

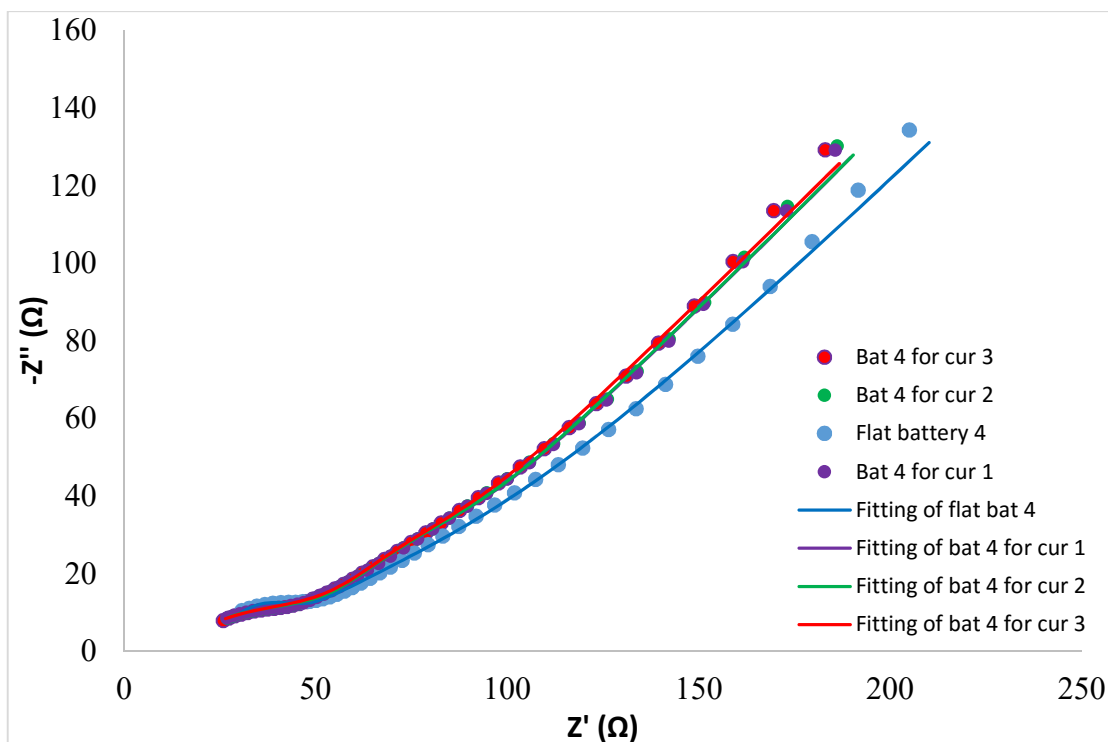


Figure 3.14 Nyquist plots of cycled Battery 4, fabricated using an electrolyte prepared with 600,000Mw PEO host.

For all the Nyquist plots of this cycled battery at different curvatures, the ohmic resistance of the first semicircle—which is the combination of electrolyte resistance and the SEI film formation resistance—has similar value compared to the Nyquist plots of previous cycled batteries. However, when it comes to the depth of first semicircle, the value of capacitances in this figure is, by comparison, smaller than the capacitances of previous cycled batteries. The slightly curved line between the electrolyte resistance and the linear diffusion line can be attributed to the combination of charge transfer resistance on the real x-axis and the double-layer capacitance on the imaginary y-axis.

This curved line has the same appearance in the last three batteries as well. The small capacitance of the potential formation of SEI or other passivation film may arise from the lack of liquid plasticizer added during the fabrication process. Figure 3.15 shows the Nyquist plot of cycled Battery 5.

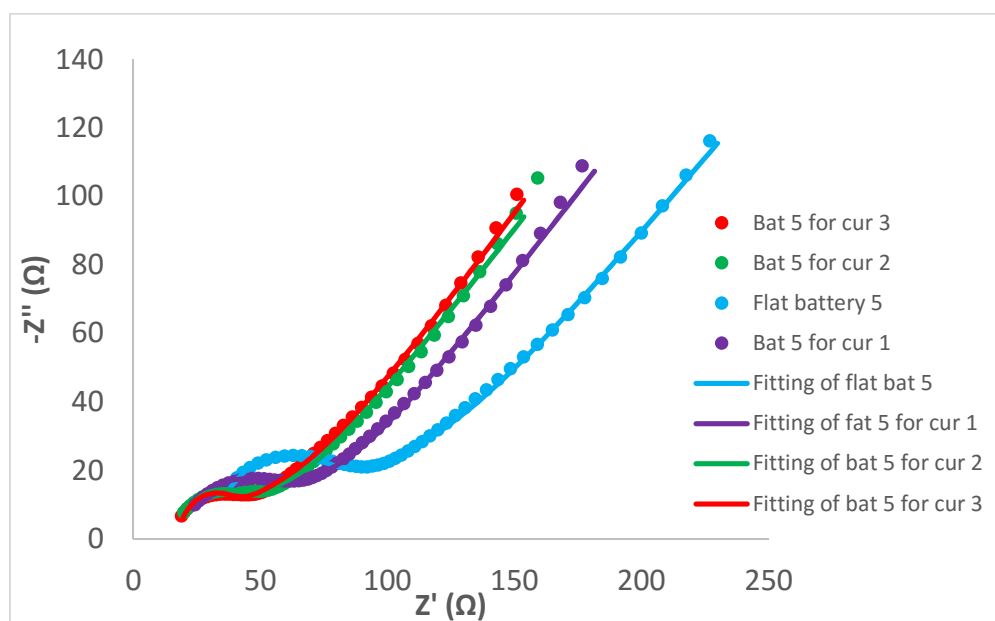


Figure 3.15 Nyquist plots of cycled battery 5, fabricated using an electrolyte prepared with 600,000Mw PEO host.

Contradictory to all previous batteries, the nyquist plots of this cycled battery appear similar to the Nyquist plot of a fresh (uncycled) battery. Generally, the Nyquist plots of cycled batteries should ideally have two semicircles. Also, each semicircle generally represents the combination of resistance and capacitance. If the impedance of a resistance and impedance of a capacitance have the values which are visible on the x and y-axis, the semicircle can be observed on the Nyquist plot. In this case, there are two possible explanations for the deviation from the general trend.

First, the two semicircles may be overlapped. Secondly, the second semicircle may not be visible due to the high ratio between the impedance of the charge transfer resistance, and the impedance of double-layer capacitance. Although the Nyquist plots of the battery show unusual behavior, it is clear that a better interfacial contact and a lower contact resistance can be achieved at the highest radius of curvature.

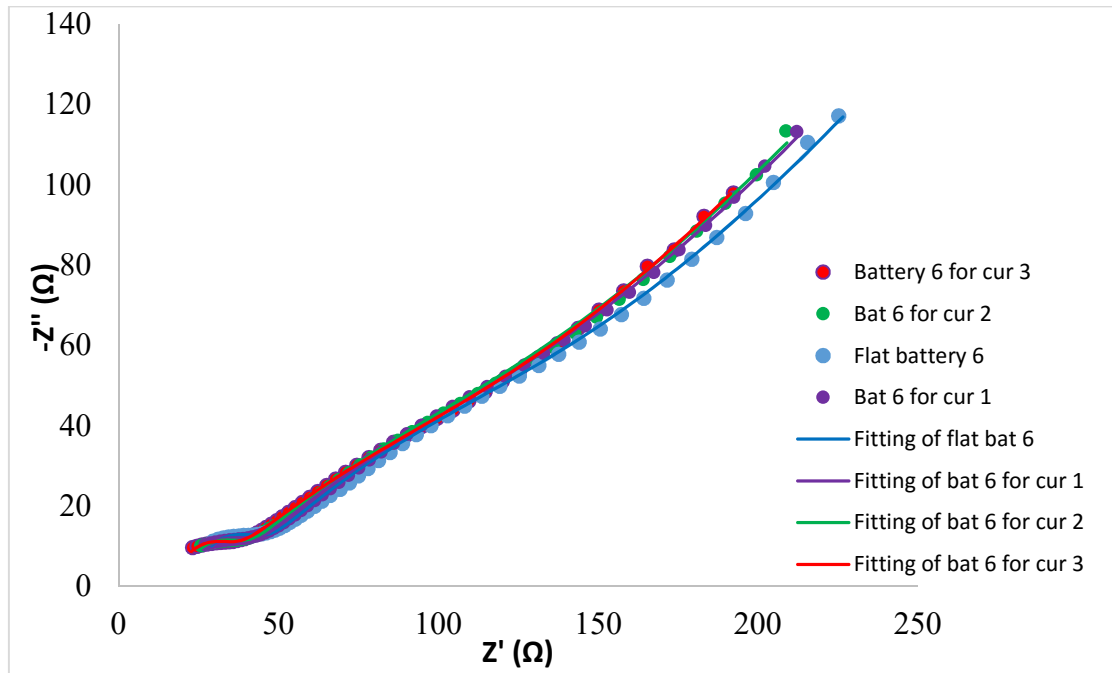


Figure 3.16 Nyquist plots of cycled Battery 6, fabricated using an electrolyte prepared with 600,000Mw PEO host.

The blue-colored plot symbolizes the actual and fitted data of the battery in flat position, the red-colored plot symbolizes the actual and fitted data of the battery for Curvature 3. By carefully examining the figure, it is noted that the red plot exhibits the lower value of contact resistance, and the blue plot shows the highest value of contact resistance.

In terms of electrolyte and charge transfer resistance, the cycled Battery 6 for Curvature 3 presents the lowest value. That means better contact may provide easier charge transfer from the cathode to the anode through the SPE.

3.3.4 Nyquist Plots of Batteries Cycled at 50 °C

The Nyquist plots of the last three batteries, cycled at 50 °C in the oven and fabricated using SPEs prepared with 100,000 Mw PEO host, are presented and discussed in this section. With increased buckling, as depicted in Figure 3.17, the interface contact and the charge transfer resistance show small amount of enhancement.

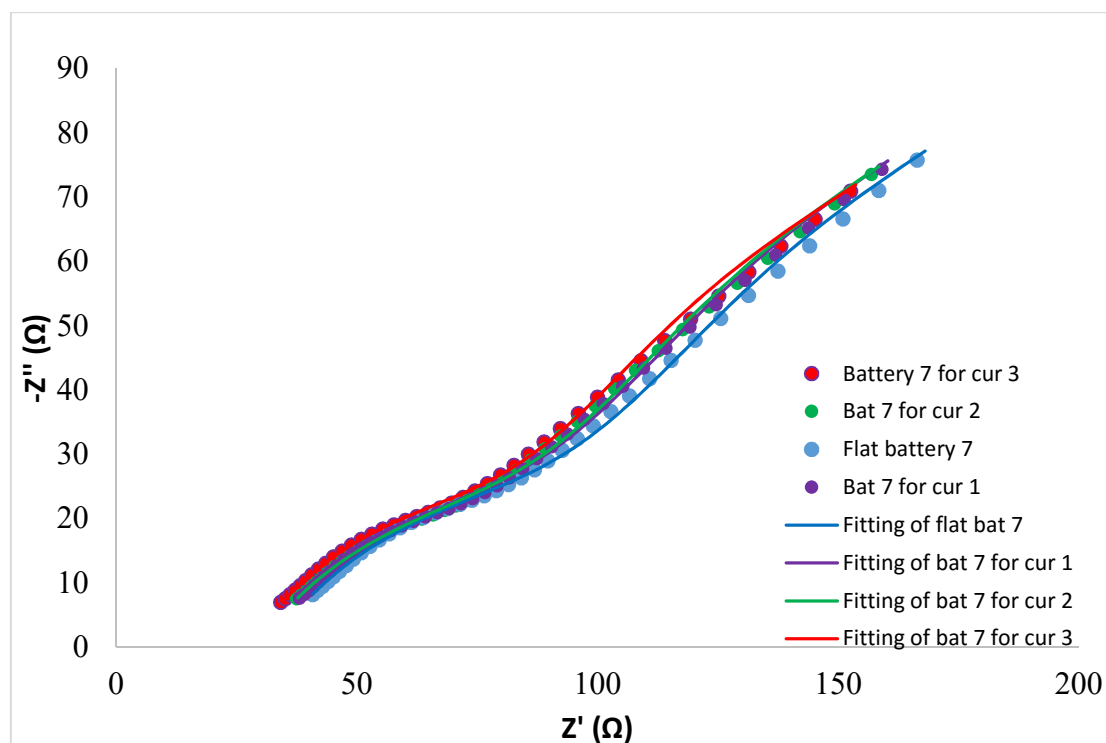


Figure 3.17 Nyquist plots of battery 7, fabricated using an electrolyte prepared with 100,000Mw PEO host and cycled in the oven.

The linear diffusion line, the capacitance (due to the SEI or passivation film) and the double-layer capacitance do not display considerable changes. Figure 3.18 depicts the Nyquist plots of Battery 8 cycled in the oven.

Although the value of the contact resistance of the cycled Batteries 7 and 8 have approximate decrease in percentages, this reduction is more observable in Figure 3.18. The potential reason to why the shifts in the values of contact resistance for the cycled Battery 8 is more obvious is because the changes in the SEI film and charge transfer (ct) resistances are relatively more drastic than the changes (SEI film and ct resistances) in the cycled Battery 7.

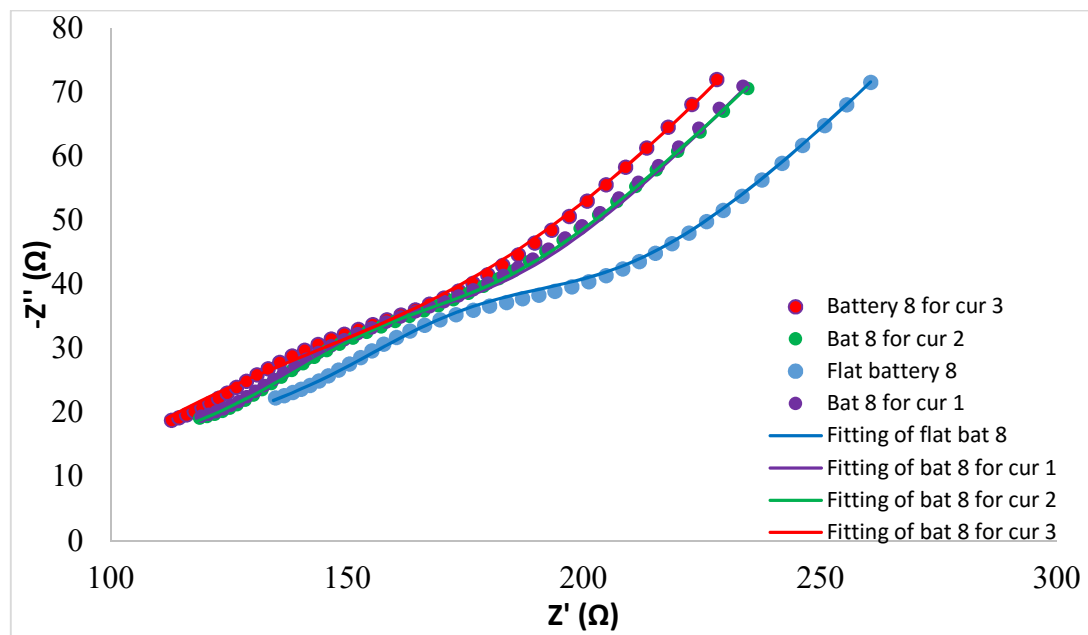


Figure 3.18 Nyquist plots of Battery 8, fabricated using an electrolyte prepared with 100,000Mw PEO host and cycled at 50 °C.

In Figure 3.19, the Nyquist plots of cycled Battery 9 at different buckling curvatures are presented. Except for the plot of the battery in flat position, all other plots appear to be overlapped in this figure. These overlapped plots representing buckled batteries for different curvatures provide an absolute advantage due to their lower resistances compared that of the flat battery. The cycled Battery 9 indicates similar characteristic behavior compared to the cycled Battery 5.

The possible reasons for exhibiting characteristic Nyquist plot of a fresh battery, as suggested previously regarding Battery 5, are also valid for Battery 9. Finally, even the contact resistances of the overlapped plots display improvement with the increasing amount of buckling as in all other cycled batteries.

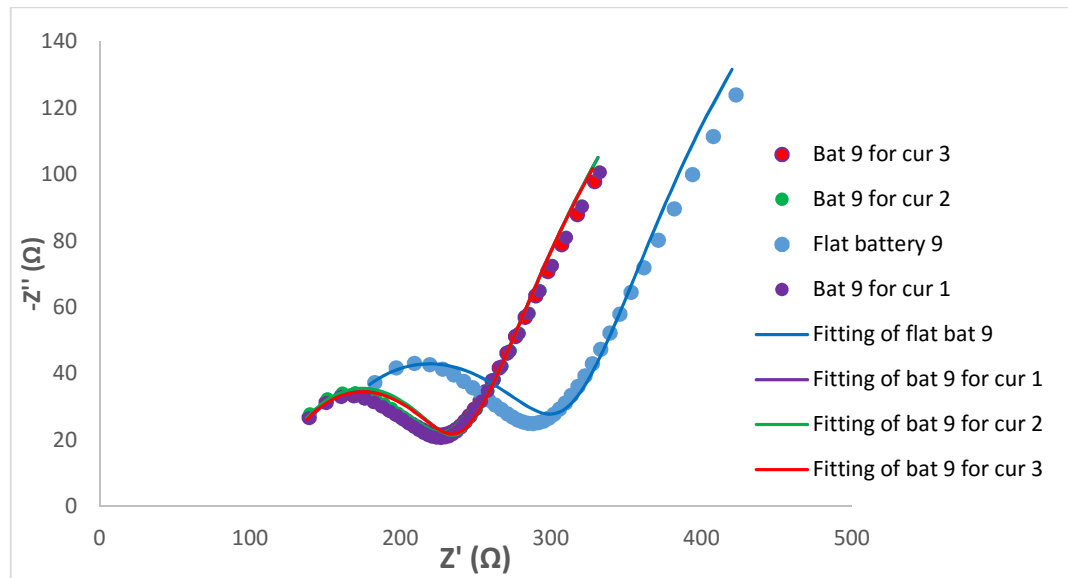


Figure 3.19 Nyquist plots of Battery 9, fabricated using an electrolyte prepared with 100,000Mw PEO host and cycled at 50 °C.

3.4 Fit and Simulation-Based Equivalent Circuits of Fresh and Cycled Batteries

The equivalent circuits (ECs) of fresh and cycled batteries used to fit the measured data collected from the EIS are presented here. The various values of the EC elements were obtained for every single battery at four different curvatures by implementing the curve fitting and simulation method.

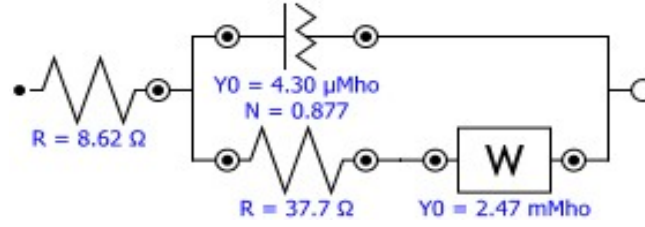


Figure 3.20 The equivalent circuit used to fit measured data of fresh batteries.

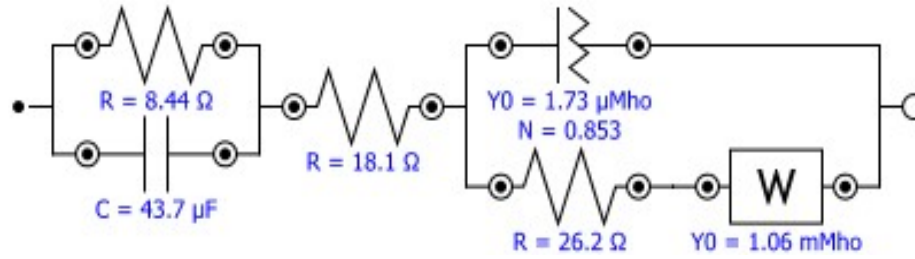


Figure 3.21 The equivalent circuit used to fit measured data of cycled batteries.

For the EC of fresh batteries, the first R represents the contact resistance and the second R represents the bulk resistance, the constant phase (Q) element can be attributed to the double-layer capacitance mechanism in the battery. For the EC of cycled batteries, the first R is for the electrolyte resistance plus the potential resistance due to the formation of the SEI or passivation film. The second R stands for the contact resistance between the components of the battery. The last R on the right side represents the charge transfer resistance. The element C is for the capacitance behavior in the battery due to potential SEI film formation, and Q represents the double-layer capacitance. All values of the resistances (R), capacitances (C), Warburg impedances and constant phase elements (Q) that are the combination of $Y0$ and N , as seen in Figure 3.20 and Figure 3.21 are presented in Tables 3.1 - 3.4.

Table 3.1 The EC elements with their values for fresh batteries, fabricated using an electrolyte prepared with 100,000Mw PEO host.

	Curvature (mm)	Rc (Ω)	R1 (Ω)	CPE (Q)	W
B a t t e r y 1	0	26.498	33.308	Y0=4.13E-06 N=0.88278	Y0=0.0002151
	0.031417	9.2915	34.481	Y0=3.70E-06 N=0.89203	Y0=0.002124
	0.032829	8.948	36.777	Y0=4.08E-06 N=0.87972	Y0=0.002315
	0.46577	8.6224	37.654	Y0=4.30E-06 N=0.87679	Y0=0.002466
B a t t e r y 2	0	58.459	40.838	Y0=3.98E-06 N=0.77239	Y0=0.00091
	0.3868	31.176	38.887	Y0=3.24E-06 N=0.8933	Y0=0.001527
	0.46757	29.53	40.2	Y0=3.20E-06 N=0.89253	Y0=0.003871
	0.53958	26.749	41.75	Y0=3.71E-06 N=0.87837	Y0=0.0015175
B a t t e r y 3	0	38.053	55	Y0=6.04E-06 N=0.8267	Y0=0.001808
	0.34965	35.101	50.7	Y0=4.32E-06 N=0.86127	Y0=0.001856
	0.40917	33.528	50	Y0=6.26E-06 N=0.82538	Y0=0.001932
	0.46296	32.463	50	Y0=5.25E-06 N=0.84423	Y0=0.001962

Table 3.2 EC elements with their values for batteries, fabricated using electrolyte prepared with 100,000Mw PEO host and cycled at room temperature.

	Curvature (mm)	R _c (Ω)	R ₁ (Ω)	R ₂ (Ω)	C (F)	CPE (Q)	W
B a t t e r y 1	0	21.156	16.925	55.141	5.33E-05	Y0=4.96E-06 N=0.75518	Y0=0.001073
	0.032	18.902	12.584	41.315	5.34E-05	Y0=4.34E-06 N=0.79253	Y0=0.001075
	0.0394	18.392	14.197	42.547	5.44E-05	Y0=5.36E-06 N=0.77493	Y0=0.001206
	0.546	16.98	14.998	44.475	5.62E-05	Y0=6.77E-06 N=0.75403	Y0=0.001399
B a t t e r y 2	0	21.65	10.959	45.611	4.87E-07	Y0=0.000188 N=0.60728	Y0=0.000931
	0.3517	18.806	9.0448	24.888	4.17E-05	Y0=1.55E-06 N=0.86507	Y0=0.001098
	0.4291	18.062	8.4364	26.178	4.37E-05	Y0=1.73E-06 N=0.85315	Y0=0.001058
	0.4973	17.676	8.2919	27.26	4.47E-05	Y0=1.82E-06 N=0.84898	Y0=0.001049
B a t t e r y 3	0	13.907	8.2221	73.156	7.43E-07	Y0=0.000356 N=0.56424	Y0=0.000848
	0.3265	12.244	9.2715	19.367	8.91E-05	Y0=2.13E-05 N=0.66764	Y0=0.001125
	0.4138	12	8.2	18.997	8.34E-05	Y0=1.95E-05 N=0.67238	Y0=0.001082
	0.5283	11.8	8.2	19.099	8.19E-05	Y0=1.67E-05 N=0.68517	Y0=0.001072

Table 3.3 EC elements with their values for batteries, fabricated using electrolyte prepared with 600,000Mw PEO host and cycled at room temperature.

	Curvature (mm)	Rc (Ω)	R1 (Ω)	R2 (Ω)	C (F)	CPE (Q)	W
B a t t e r y 4	0	22.502	14.014	114.22	2.05E-07	Y0=0.000279 N=0.4742	Y0=0.000433
	0.03370976	12.341	10.507	48.087	4.65E-05	Y0=5.74E-05 N=0.49278	Y0=0.000649
	0.04192169	11.909	9.749	50	5.13E-05	Y0=7.00E-05 N=0.47583	Y0=0.000636
	0.05400734	11.654	7.9423	52	6.95E-05	Y0=9.39E-05 N=0.45928	Y0=0.000628
B a t t e r y 5	0	24.743	29.096	116.31	2.10E-07	Y0=0.000376 N=0.39601	Y0=0.000479
	0.031785	18.784	25.547	51.763	3.70E-07	Y0=0.000153 N=0.57668	Y0=0.000745
	0.040865	18.05	17.95	45.927	4.74E-07	Y0=0.000228 N=0.46261	Y0=0.000665
	0.048726	16.686	17.412	48.781	5.34E-07	Y0=0.000157 N=0.44738	Y0=0.000698
B a t t e r y 6	0	22.109	15.78	123.456	1.83E-07	Y0=0.000173 N=0.53164	Y0=0.000677
	0.03295436	20.299	14.293	99.88	2.09E-07	Y0=0.000225 N=0.51211	Y0=0.000662
	0.04142674	18.475	13.313	99.14	2.08E-07	Y0=0.000256 N=0.49828	Y0=0.000656
	0.05138482	15.969	12.345	94.05	2.27E-07	Y0=0.000328 N=0.47356	Y0=0.00072

Table 3.4 EC elements with their values for batteries, fabricated using electrolyte prepared with 100,000Mw PEO host and cycled at 50 °C.

	Curvature (mm)	Rc (Ω)	R1 (Ω)	R2 (Ω)	C (F)	CPE (Q)	W
B a t t e r y 7	0	31.809	30.59	84.329	6.21E-05	Y0=5.80E-05 N=0.53503	Y0=0.000544
	0.03286339	29.758	29.866	82.748	6.71E-05	Y0=6.74E-05 N=0.52996	Y0=0.000549
	0.04058936	29.145	29.04	81.203	6.59E-05	Y0=7.06E-05 N=0.52537	Y0=0.000548
	0.05190141	27.719	29.103	72.407	5.97E-05	Y0=4.52E-05 N=0.57056	Y0=0.000593
B a t t e r y 8	0	64.686	15.585	196.39	1.24E-06	Y0=0.000249 N=0.26957	Y0=0.000129
	0.03183	63.5	12.466	160.25	1.72E-06	Y0=0.000238 N=0.53503	Y0=0.000125
	0.04003	60.979	11.831	175.42	1.90E-06	Y0=0.000318 N=0.26871	Y0=0.00011
	0.046922	60	17.697	153.94	9.00E-13	Y0=5.80E-05 N=0.53503	Y0=0.000166
B a t t e r y 9	0	124.24	66.379	182.5	3.56E-05	Y0=1.99E-06 N=0.55006	Y0=0.000275
	0.03438908	109.66	38.281	126.03	5.75E-05	Y0=1.07E-06 N=0.63079	Y0=0.000319
	0.04144219	108.28	36.418	126.9	6.13E-05	Y0=9.44E-07 N=0.63658	Y0=0.0003156
	0.04913619	106.67	40.117	130.08	5.71E-05	Y0=1.43E-06 N=0.0.60799	Y0=0.000334

3.5 Resistance and Conductance at Different Buckling Curvatures

In this section, for every tested battery, the changes in total resistance and conductance at different buckling curvatures are presented. In addition, in the subsection, the normalized contact conductance of each tested battery is discussed. All resistances for each parameter were given previously in Tables 3.1 to 3.4. Also, in the previous sections, the Nyquist plots of the batteries demonstrated the values of resistances with the various amount of buckling.

3.5.1 Total Resistance and Total Conductance for Different curvatures

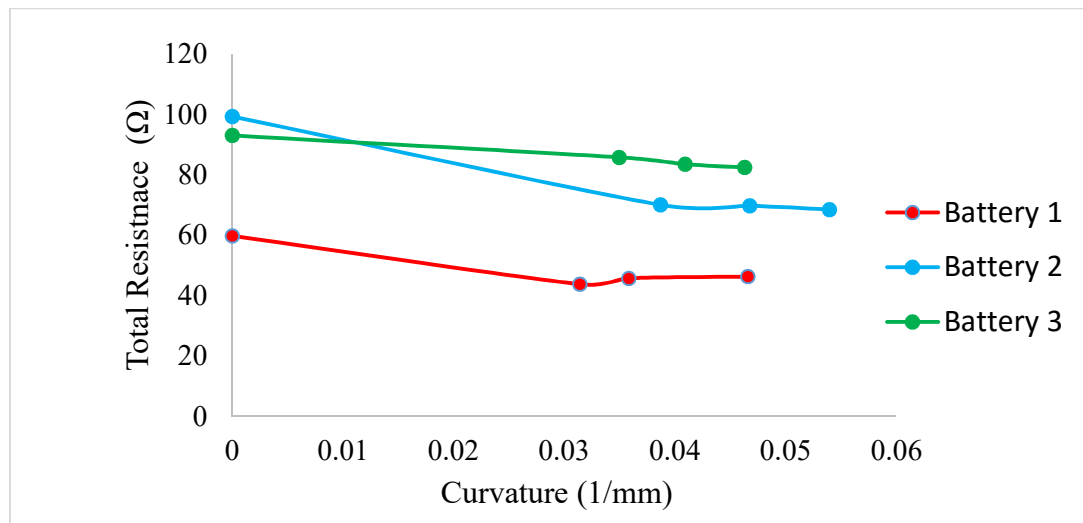


Figure 3.22 Total resistance of fresh batteries.

For the fresh Batteries 2 and 3, the total resistances decrease continuously with increasing radius of curvature. For Battery 1, the buckled battery has a clear advantage over the battery in flat position. However, after the first buckling curvature, the total resistance slightly increases. The cause of this increase may be the beginning of the delamination process with further buckling.

In other words, slight bending/buckling of the flexible battery may offer enhanced interlayer contact, however, further bending/buckling can lead to adverse effects including delamination.

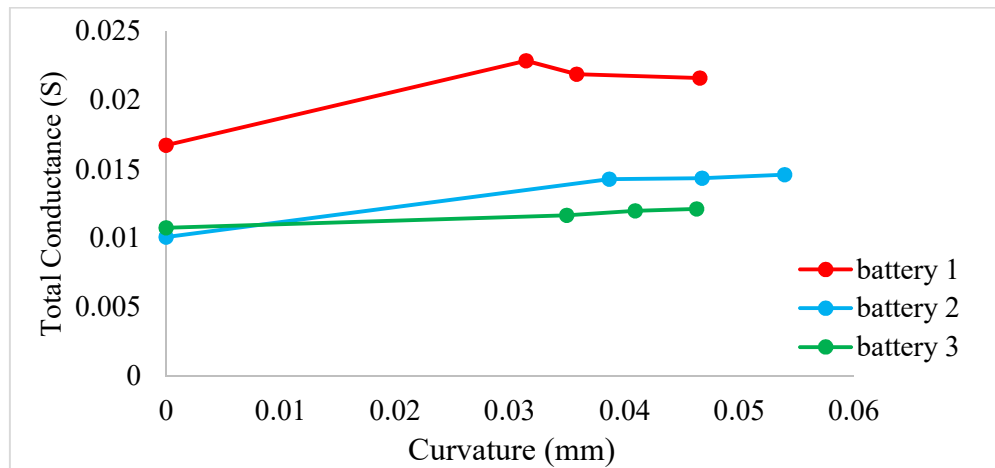


Figure 3.23 Total conductance of fresh batteries.

Figure 3.23 shows the changes in the total conductance of the fresh batteries. Since conductance is an inverse of resistance ($1/\text{resistance}$), total conductance of fresh Battery 2 and Battery 3 increases continuously, and contact conductance of Battery 1 exhibits a slight decline with further buckling after Curvature 1.

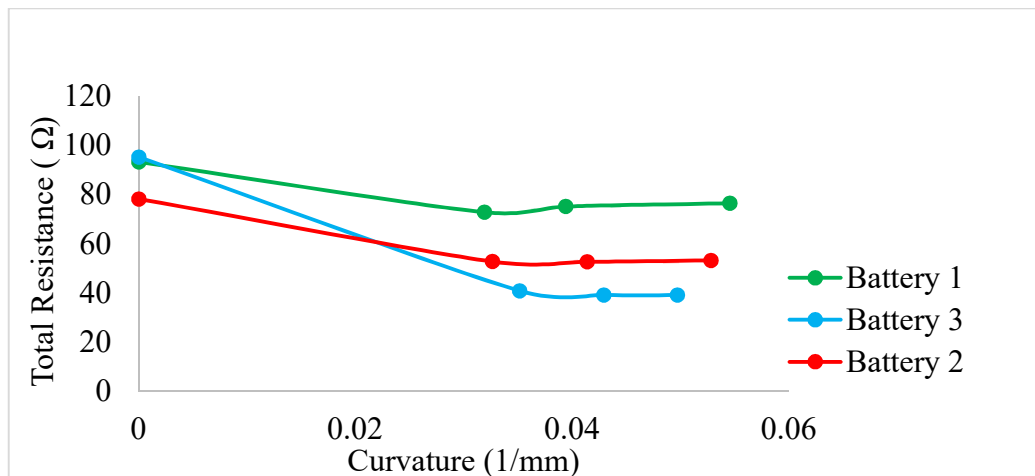


Figure 3.24 Total resistances of cycled Batteries 1, 2 and 3.

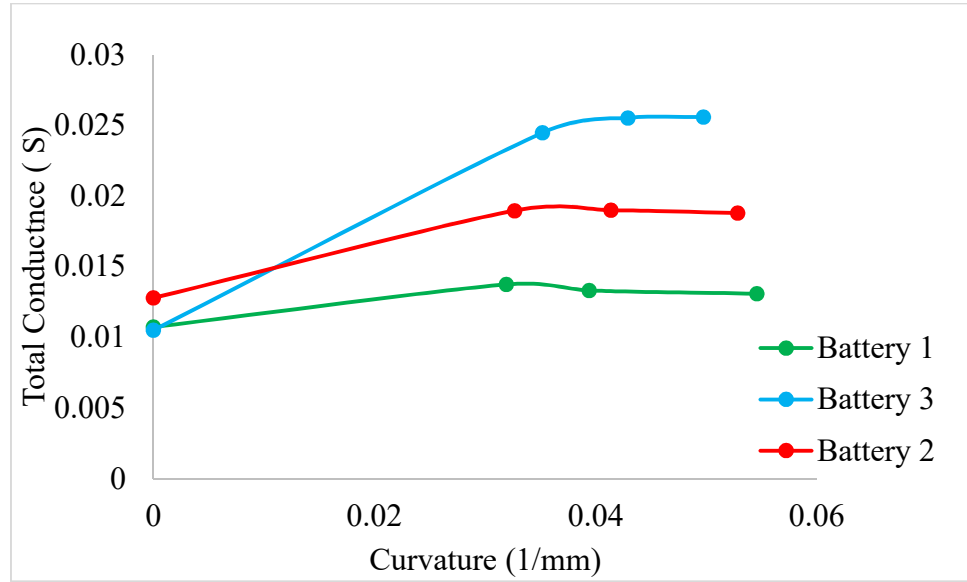


Figure 3.25 Total conductance of cycled Batteries 1, 2 and 3.

For the cycled Batteries 1, 2 and 3 in Figure 3.24 and Figure 3.25, the total resistances decrease with the first buckling curvature. By applying the second and third buckling curvatures, the contact resistance of Battery 3 still decreases, while the conductance of Battery 3 increases. On the other hand, Battery 1 and Battery 2 exhibit slight increase in the total resistance with Curvatures 2 and 3. Nevertheless, at all three buckling curvatures, the total conductance of Batteries 2 and 3 is higher than the conductance of the unbuckled (flat) battery. That further proves that the buckling up to a certain radius can improve the performance of the batteries by decreasing the total resistance. Lastly, increase in the total conductance is the highest for Battery 3 because of the highest decline in the value of charge transfer resistance. This can be seen in Table 3.2. For the evaluation of these batteries, all concatenated reasons for the previous three batteries are valid for the cycled Battery 4, Battery 5 and Battery 6 whose changes in conductance and resistance are given in Figure 3.26 and Figure 3.27.

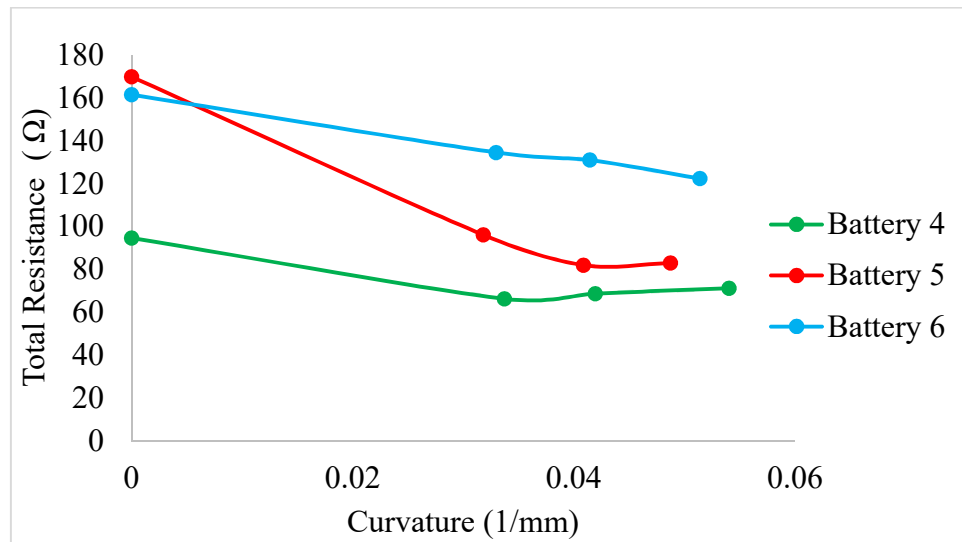


Figure 3.26 Total resistances of cycled Batteries 4, 5 and 6.

The conductance of Battery 6 appears to consistently rise up with increased buckling. For Battery 4 and Battery 5 after certain radius, the value of conductance shows a slight drop.

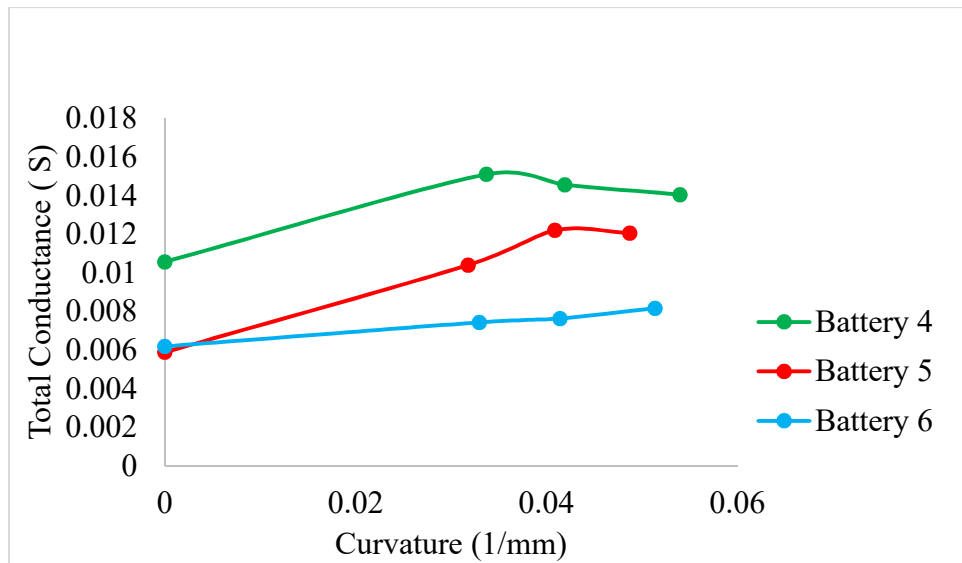


Figure 3.27 Total conductance of cycled Batteries 4, 5 and 6.

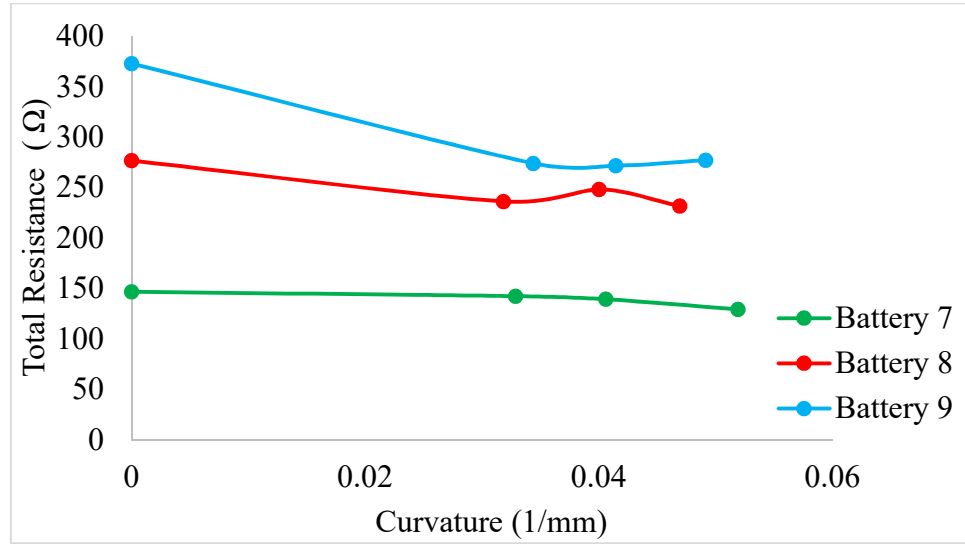


Figure 3.28 Total resistances of cycled Batteries 7, 8 and 9.

In Figure 3.28 and Figure 3.29, the last three cycled batteries show enhancement in terms of total conductance and total resistances. Although there are fluctuations in the value of conductance for the different curvatures, all batteries under buckling have considerably higher total conductance values over flat batteries. That confirms that usually buckling up to certain radius of curvature leads to preferable conductance and resistance.

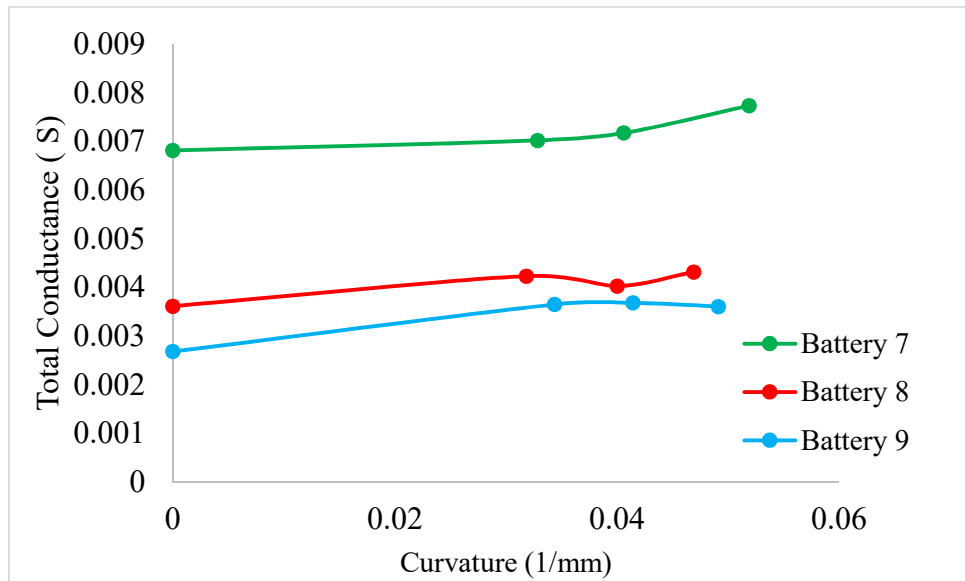


Figure 3.29 Total conductance of cycled Batteries 7, 8 and 9.

3.5.2 Normalized Contact Conductance for Different Curvatures

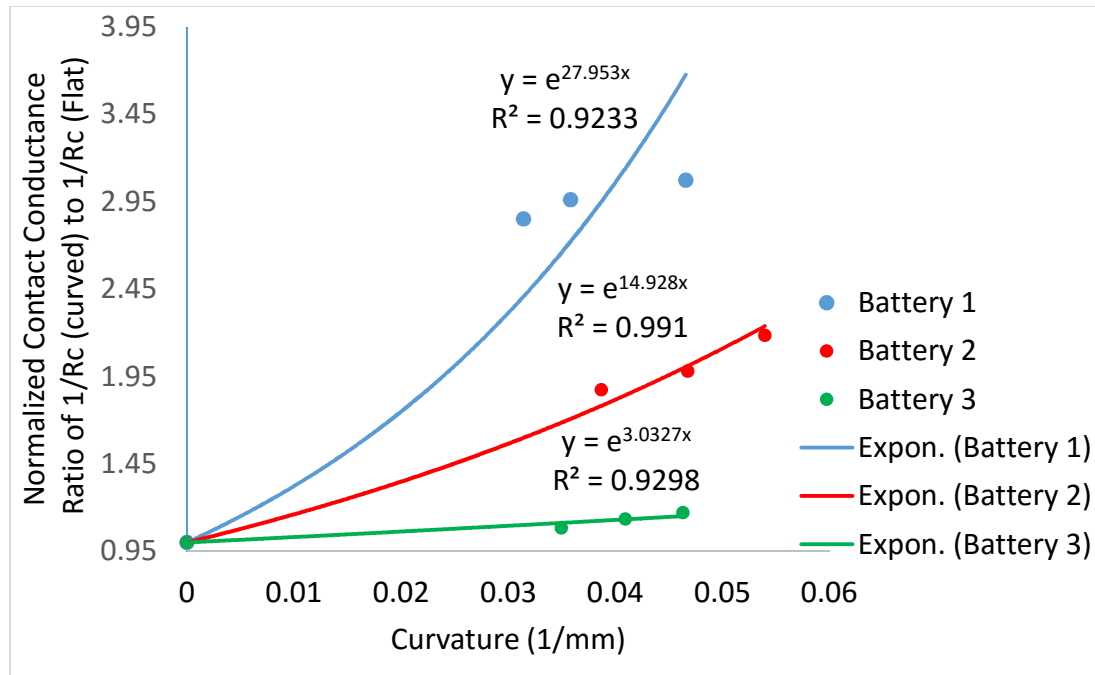


Figure 3.30 Normalized contact conductance of fresh battery 1, battery2 and battery 3 at different curvatures.

In Figure 3.30, the normalized contact conductance demonstrates exponential growth for all three fresh batteries with the increasing value of radius of curvature. However, these growths vary due to changes between the interface of the components in flat position and the interface under buckling at different curvatures. Battery 3 is the most stable battery under buckling. It can be assumed based on the plots that at the beginning, Battery 3 had better interface contact than that of other fresh batteries. All plots for the three different fresh batteries demonstrate that with the higher amount of buckling, fresh batteries are inclined to have better interfaces and higher conductance.

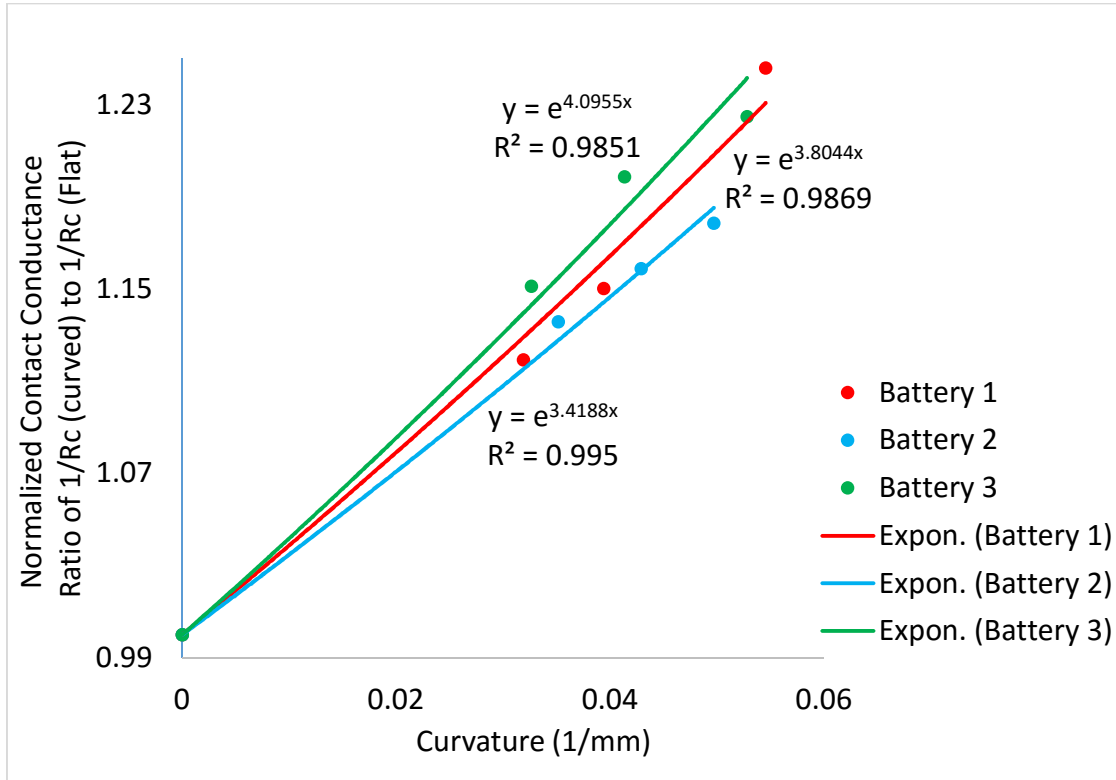


Figure 3.31 Normalized contact conductance of battery 1, battery 2 and battery 3 cycled at room temperature and tested at room temperature under different buckling curvatures.

Normalized contact conductance of cycled batteries in Figure 3.31 shows approximate exponential growths for all three batteries. This may result from the cycling process applied to the batteries before EIS measurements because the cycling process, due to the heat, leads to plasticization of electrolyte which can cause better interfaces between components of batteries. The battery with better interfaces between its components in flat position generally has smaller amount of exponential growth in contact conductance under buckling than the battery with the weaker interface between its components. Cycled batteries using different SPE in Figure 3.32 does not act in same particular manner as in Figure 3.31.

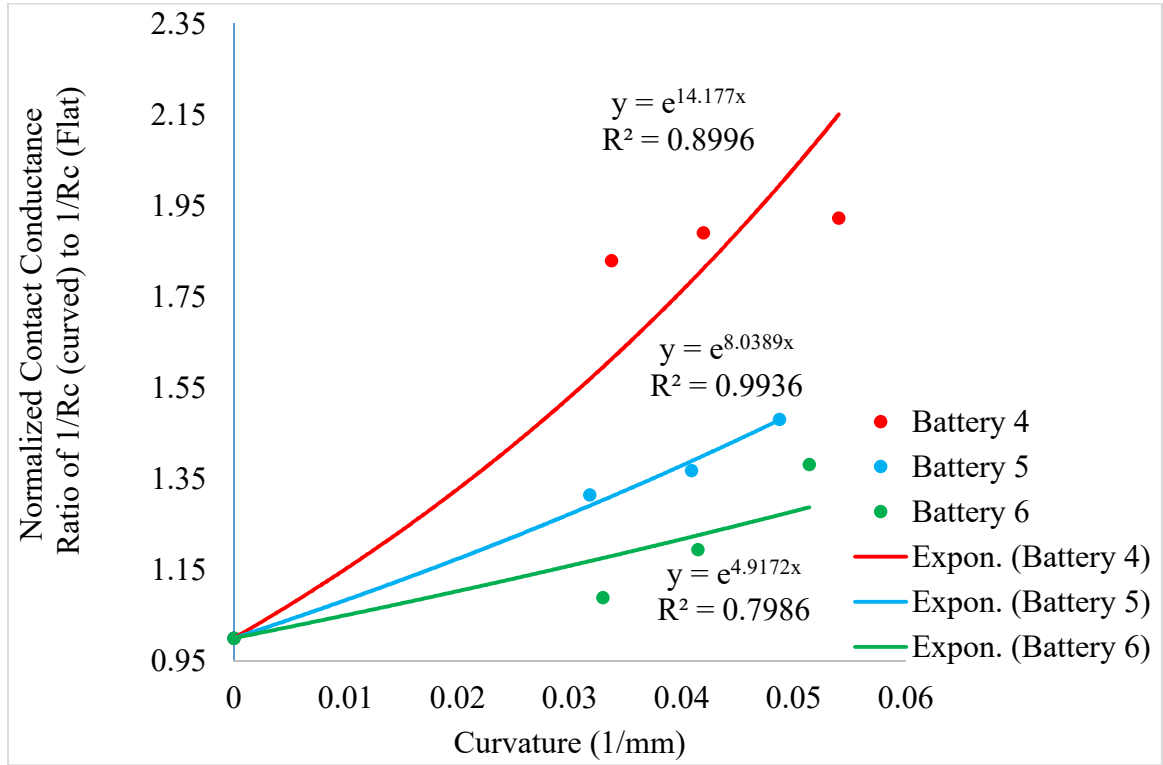


Figure 3.32 Normalized contact conductance of batteries using an electrolyte prepared with 600,000 Mw PEO, cycled and tested at room temperature under different buckling curvatures.

Several assumptions can be made for different amount of exponential changes of each battery buckled at different curvatures. First of all, the liquid electrolyte added on the surface of both electrodes during the fabrication process may be slightly lower for Battery 4. Secondly, good match of layers may not have been achieved during the fabrication process or during the laminating process for the Battery 4. Finally, SPEs prepared with 600,000 Mw PEO host may have weaker interface contact than SPEs prepared with 100,000 Mw PEO host. This can be attributed to the material properties of those electrolytes. Compared to the first cycled batteries in Figure 3.31, Battery 5 in Figure 3.32 also exhibits a large change in contact conductance.

Therefore, the assumptions made above can be valid for cycled Battery 5 as well. Battery 6 of Figure 3.32 displays similar behavior to the batteries in the previous figure.

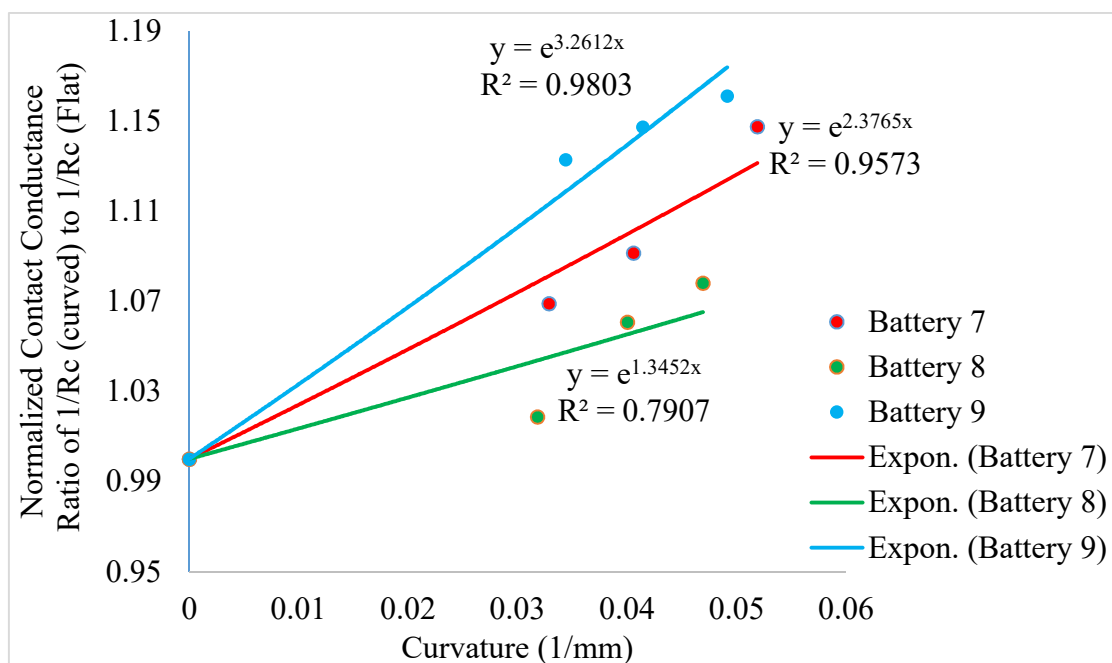


Figure 3.33 Normalized contact conductance of batteries cycled at 50°C and tested at room temperature under different buckling curvatures.

According to the EIS measurements, the batteries cycled in the oven at 50 °C are the most stable batteries in terms of contact resistances and contact conductance. Exponential changes of each battery in the figure show similar increases with the higher values of curvature. As mentioned earlier, those batteries are cycled at 50°C and are immediately tested after the cycling process at room temperature. Possibly, at 50°C, SPEs of these batteries had a better contact with anode and cathode due to the plasticization of the polymer at higher temperature.

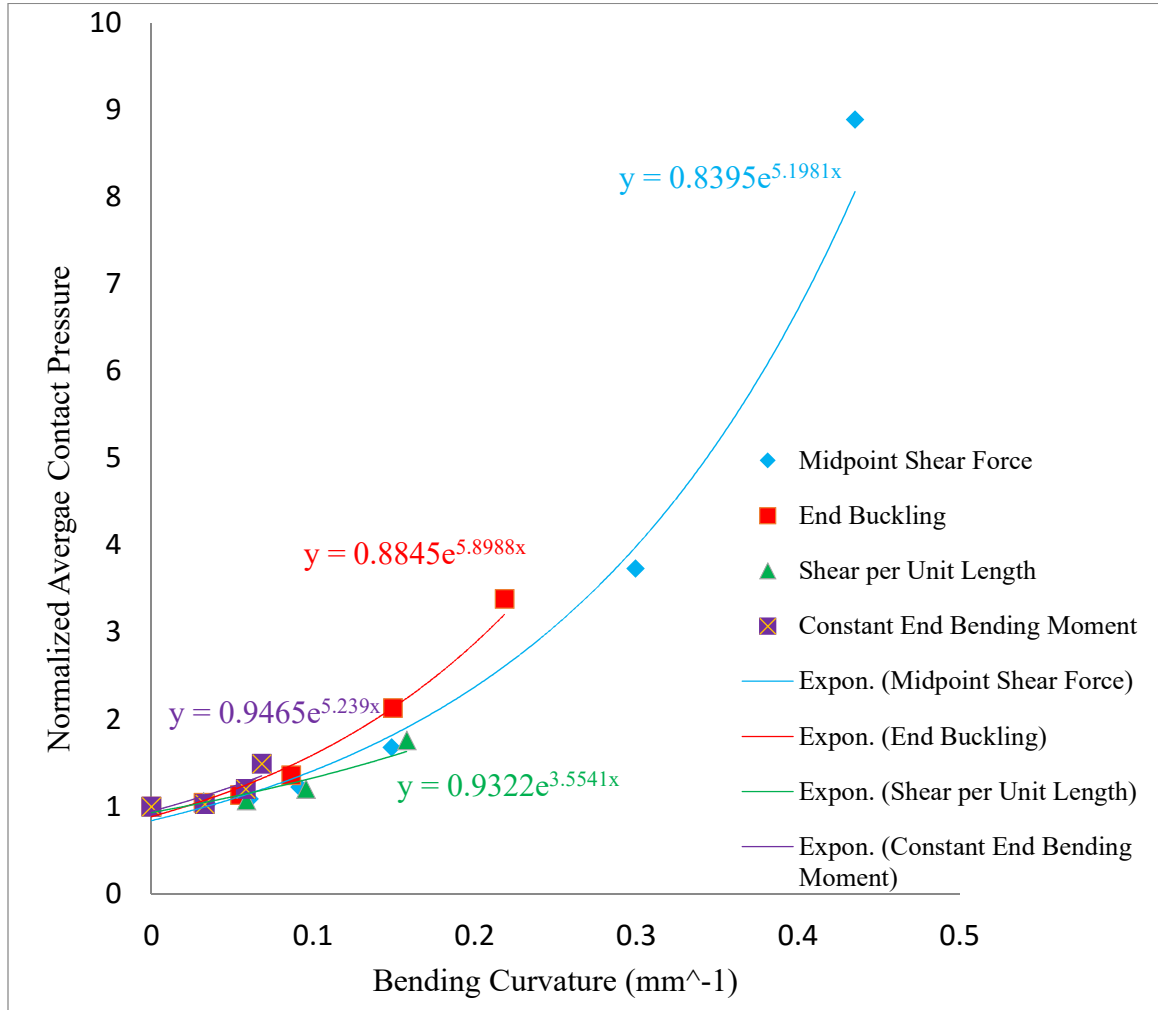


Figure 3.34 Plot of the average contact pressure change with increasing curvature based on the numerical study conducted by Sean Berg [41].

In this numerical study [41], basically, the interfacial contact pressure between the electrolyte and electrode interfaces in solid polymer electrolyte flexible LIBs under different types of bending methods are investigated. Flexible LIB was considered as a composite multi-layer structure. It is assumed that the delamination of the layers under mechanical loading were prevented by applying surface pressure on the top and bottom layers of structure with lamination as in experimental study.

For each bending method, it was observed that the contact pressure increases nonlinearly with the increase in the radius of curvature. The variation in the trends of different bending/buckling methods could arise from the geometric profile of the battery under loading, the approximate estimations of the material properties, and the basic assumptions made in the numerical model. It is accepted that the contact pressure of the battery has direct relationship with the contact conductance. End buckling numerical method used in Figure 3.34 verifies the results of the experimental study. Basically, with increasing radius of curvature, the contact conductance obtained experimentally for the cycled battery (fabricated based on SPE using 100,000 Mw) shows similar exponential growth behavior as that observed from the numerical study of the increase in contact pressure of the battery exposed to end buckling.

Chapter 4 Conclusions and Future Work

4.1 Conclusions

In this study, the effects of buckling on the interface contact impedance in flexible Li-ion batteries were investigated. The flexible batteries fabricated in this study were thin-film batteries made with solid polymer electrolyte. Specifically, two types of nanocomposite solid polymer electrolytes prepared with 1% graphene oxide embedded in 100,000 Mw polyethylene oxide (PEO) host and with 1% graphene oxide embedded in 600,000 Mw PEO host were used in the fabrication of flexible lithium ion batteries. Batteries encapsulated with scalable and economical lamination process, offer good electrochemical performance and large-range functionality under mechanical deformation. Buckling experiments on fabricated flexible lithium ion batteries using nanocomposite polymer electrolytes were performed to provide further insight about the battery characteristics under loading. The focus of this study, in particular, was to evaluate the change in the contact resistance of the components of fresh and cycled batteries under different buckling curvatures. Electrochemical impedance spectroscopy (EIS) technique was used to investigate the impedance of the flexible lithium ion batteries. Fresh batteries were buckled to different curvatures over 10 to 20 charge/discharge cycles. The three different fresh batteries tested under buckling exhibited slightly different characteristics. Fresh Battery 1 exhibited approximately two folds ($26.4\ \Omega$ to $8.9\ \Omega$) decline in contact resistance from flat position to the highest buckling curvature.

However, there was a slight increase in bulk resistance ($33.3\ \Omega$ to $37.8\ \Omega$) of the fresh Battery 1. Fresh Battery 2 has demonstrated 119 % ($58.4\ \Omega$ to $26.7\ \Omega$) enhancement in contact resistance and contact conductance, and has also exhibited $0.9\ \Omega$ increase in bulk resistance. Fresh Battery 3 was the most stable battery in terms of contact resistance and contact conductance. The decrease in contact resistance was around $6\ \Omega$. In addition, the bulk resistance decreases in value of $5\ \Omega$. Improvement in contact resistances of the first three cycled batteries (Battery 1, 2 and 3) under buckling were relatively moderate and were between 17% and %24. For the highest value of radius of curvature, these batteries had the lowest value in contact resistance. Also, the total resistances of these three cycled batteries reduced compared to that in flat position. Cycled Batteries 4, 5 and 6 fabricated using an electrolyte prepared with 600,000Mw PEO host acted similarly towards buckling but with different enhancement values. The reduction in contact resistances were up to %27 for Battery 3, %48 for Battery 2 and %93 for Battery 1 from flat position to the highest value of buckling curvature. Under different buckling curvatures, batteries show considerable decline in total resistances as well. Batteries cycled in the oven exhibited most consistent behaviors under buckling in terms of contact resistance. These last cycled batteries improved contact resistance between %7 and %17 with the increasing amount of buckling. Overall, batteries under buckling clearly have an advantage over flat batteries, as they were able to provide better interface contact and contact pressure among the components of the batteries. Furthermore, usually, with the higher value of radius of curvature, lower contact resistance values were obtained. Cycled batteries, at first, were inclined to have better interfaces and showed less improvement in contact resistances than fresh batteries.

However, interface between the components of fresh Battery 3 was as good as the cycled batteries. This can be attributed to a good adhesion between the thin components during the fabrication process or the addition of slightly more liquid plasticizer during the fabrication process. Batteries based on SPEs with 100,000 Mw PEO host initially had better interface than batteries based on SPEs with 600,000 Mw PEO host. According to the experimental results, batteries cycled in the oven at 50°C, have best initial interfaces and less improvement in contact resistances are achieved with buckling. The following reasons can cause better initial interfaces: (1) Solid polymer nanocomposite electrolytes plasticizes at higher temperatures; (2) the effect of liquid plasticizer added during the fabrication increases with higher temperatures; and (3) enhanced diffusion and transport of species due to higher temperature improves the impedance values in the battery.

4.2 Future Work

Conventional lithium ion batteries based on organic liquid electrolytes have rigid bodies and design limitations. Flexible lithium ion batteries can overcome these design limitations and can lead to revolutionary new designs in industry by their integration to the portable electronics, flexible consumer electronics, clothes, glasses, watches and skin devices. Foldable and bendable capabilities of flexible lithium ion batteries will lead to new designs of thin and light weight flexible electronics. Creative smart clothes that have different functionalities such as winter clothing that keeps people warm or summer clothing that keep people cold can be produced by implementation of flexible batteries to the textiles. There is a growing interest for the virtual reality glasses. Although few virtual reality glasses were released to the market successfully, their large sizes and heavy weights restricts their usage.

Besides, light and small-sized virtual reality glasses, enhanced glasses for visual impairment can be rendered possible by flexible lithium ion batteries embedded in frames of glasses. Furthermore, for either smartwatches or multifunctional watches with the high energy consumption, embedding of flexible battery into watchstraps can increase hours of usage per charging. Finally, since health care is one of the most important subjects for human beings, therefore, the medical implants and health-monitoring skin devices will never fall from grace. By the compatibility of flexible batteries with the skin, the smart devices can warn and guide people before a heart attack or a change in blood pressure. Furthermore, smart devices can measure the blood glucose level automatically at a set time and keeping track. All these ambitious functions of smart devices can be more effectively enabled with flexible batteries that are compatible with human organs.

Investigating the optimum bending/buckling of a flexible battery that leads to maximum contact enhancement and minimum delamination can be pursued in future studies. Total resistances of the batteries display reduction at buckled position compared to flat position. However, under bending/buckling, based on the results of the experiments, the charge transfer resistance and electrolyte resistance of some batteries exhibit decline up to certain radius of curvatures; some other batteries show slight increase in charge transfer resistance or electrolyte resistance with the higher amount of buckling. The mechanism behind the changes in charge transfer and electrolyte resistance can be elucidated by focusing on those resistances in future studies. Batteries cycled at high temperature clearly shows high capacities and better contact; the effect of increase in ionic conductivity or the effect of increase in contact conductance should be investigated for high temperature operations.

Batteries based on 600,000 Mw PEO show relatively weaker initial interfaces and exhibit more reduction in contact resistance upon buckling; investigation of the relation between the material properties of 600,000 Mw PEO and the contact pressure of the battery with finite element analysis can be useful to understand the change in contact conductance of these batteries. Also, the reason why cycled batteries have less enhancement in contact conductance than the fresh batteries can be studied by cross-sectioning the cycled and fresh batteries and observing the internal structures of the batteries.

References

- [1] Ende, D. V. D., Wiel, H. V. D., Kusters, R., Sridhar, A., Schram, J., Cauwe, M., and Brand, J. V. D., 2014, “Mechanical and Electrical Properties of Ultra-Thin Chips and Flexible Electronics Assemblies During Bending,” *Microelectronics Reliability*, 54(12), pp. 2860–2870.
- [2] Cai, J., Cizek, K., Long, B., Mcaferty, K., Campbell, C. G., Allee, D. R., Vogt, B. D., Belle, J. L., and Wang, J., 2009, “Flexible Thick-Film Electrochemical Sensors: Impact of Mechanical Bending and Stress on the Electrochemical Behavior,” *Sensors and Actuators B: Chemical*, 137(1), pp. 379–385.
- [3] Sluis, O. V. D., Engelen, R., Timmermans, P., and Zhang, G., 2009, “Numerical Analysis of Delamination and Cracking Phenomena in Multi-Layered Flexible Electronics,” *Microelectronics Reliability*, 49(8), pp. 853–860.
- [4] Lewis, J., 2006, “Material Challenge for Flexible Organic Devices,” *Materials Today*, 9(4), pp. 38–45.
- [5] Münzenrieder, N., Zysset, C., Petti, L., Kinkeldei, T., Salvatore, G. A., and Tröster, G., 2013, “Room Temperature Fabricated Flexible NiO/IGZO pn Diode Under Mechanical Strain,” *Solid-State Electronics*, 87, pp. 17–20.
- [6] Zhang, P., Qiu, J., Zheng, Z., Liu, G., Ling, M., Martens, W., Wang, H., Zhao, H., and Zhang, S., 2013, “Free-Standing and Bendable Carbon Nanotubes/TiO₂ Nanofibres Composite Electrodes for Flexible Lithium Ion Batteries,” *Electrochimica Acta*, 104, pp. 41–47.
- [7] Rogers, J. A., Someya, T., and Huang, Y., 2010, “Materials and Mechanics for Stretchable Electronics,” *Science*, 327(5973), pp. 1603–1607.

- [8] Dahiya, R. S., and Gennaro, S., 2013, “Bendable Ultra-Thin Chips on Flexible Foils,” *IEEE Sensors J. IEEE Sensors Journal*, 13(10), pp. 4030–4037.
- [9] Koo, M., Park, K.-I., Lee, S. H., Suh, M., Jeon, D. Y., Choi, J. W., Kang, K., and Lee, K. J., 2012, “Bendable Inorganic Thin-Film Battery for Fully Flexible Electronic Systems,” *Nano Letters Nano Lett.*, 12(9), pp. 4810–4816.
- [10] Cetinkaya, T., Ozcan, S., Uysal, M., Guler, M. O., and Akbulut, H., 2014, “Free-Standing Flexible Graphene Oxide Paper Electrode for Rechargeable Li–O₂ Batteries,” *Journal of Power Sources*, 267, pp. 140–147.
- [11] Li, N., Chen, Z., Ren, W., Li, F., and Cheng, H.-M., 2012, “Flexible Graphene-Based Lithium Ion Batteries with Ultrafast Charge and Discharge Rates,” *Proceedings of the National Academy of Sciences*, 109(43), pp. 17360–17365.
- [12] Gwon, H., Hong, J., Kim, H., Seo, D.-H., Jeon, S., and Kang, K., 2014, “Recent Progress on Flexible Lithium Rechargeable Batteries,” *Energy Environ. Sci.*, 7(2), pp. 538–551.
- [13] Kim, B.-J., Shin, H.-A.-S., Choi, I.-S., and Joo, Y.-C., 2011, “Electrical Failure and Damage Analysis of Multi-Layer Metal Films on Flexible Substrate During Cyclic Bending Deformation,” *18th IEEE International Symposium on the Physical and Failure Analysis of Integrated Circuits (IPFA)*.
- [14] Lin, H., Weng, W., Ren, J., Qiu, L., Zhang, Z., Chen, P., Chen, X., Deng, J., Wang, Y., and Peng, H., 2013, “Twisted Aligned Carbon Nanotube/Silicon Composite Fiber Anode for Flexible Wire-Shaped Lithium-Ion Battery,” *Adv. Mater. Advanced Materials*, 26(8), pp. 1217–1222.

- [15] Xu, S., Zhang, Y., Cho, J., Lee, J., Huang, X., Jia, L., Fan, J. A., Su, Y., Su, J., Zhang, H., Cheng, H., Lu, B., Yu, C., Chuang, C., Kim, T.-I., Song, T., Shigeta, K., Kang, S., Dagdeviren, C., Petrov, I., Braun, P. V., Huang, Y., Paik, U., and Rogers, J. A., 2013, “Stretchable Batteries with Self-Similar Serpentine Interconnects and Integrated Wireless Recharging Systems,” *Nature Communications Nat Comms*, 4, p. 1543.
- [16] Kammoun, M., Berg, S., and Ardebili, H., 2015, “Flexible Thin-Film Battery Based on Graphene-Oxide Embedded in Solid Polymer Electrolyte,” *Nanoscale*, 7(41), pp. 17516–17522.
- [17] Yuan, M., Erdman, J., Tang, C., and Ardebili, H., 2014, “High Performance Solid Polymer Electrolyte with Graphene Oxide Nanosheets,” *RSC Adv.*, 4(103), pp. 59637–59642.
- [18] Scrosati, B., and Garche, J., 2010, “Lithium Batteries: Status, Prospects and Future,” *Journal of Power Sources*, 195(9), pp. 2419–2430.
- [19] Zhou, S., and Bongiorno, A., 2013, “Origin of the Chemical and Kinetic Stability of Graphene Oxide,” *Sci. Rep. Scientific Reports*, 3.
- [20] Manthiram, A., 2011, “Materials Challenges and Opportunities of Lithium Ion Batteries,” *J. Phys. Chem. Lett. The Journal of Physical Chemistry Letters*, 2(3), pp. 176–184.
- [21] Guo, J., Sun, A., Chen, X., Wang, C., and Manivannan, A., 2011, “Cyclability Study of Silicon–Carbon Composite Anodes for Lithium-Ion Batteries Using Electrochemical Impedance Spectroscopy,” *Electrochimica Acta*, 56(11), pp. 3981–3987.

- [22] Dees, D., Gunen, E., Abraham, D., Jansen, A., and Prakash, J., 2005, “Alternating Current Impedance Electrochemical Modeling of Lithium-Ion Positive Electrodes,” *Journal of The Electrochemical Society J. Electrochem. Soc.*, 152(7).
- [23] Andre, D., Meiler, M., Steiner, K., Walz, H., Soczka-Guth, T., and Sauer, D., 2011, “Characterization of High-Power Lithium-Ion Batteries by Electrochemical Impedance Spectroscopy. II: Modelling,” *Journal of Power Sources*, 196(12), pp. 5349–5356.
- [24] Andre, D., Meiler, M., Steiner, K., Wimmer, C., Soczka-Guth, T., and Sauer, D., 2011, “Characterization of High-Power Lithium-Ion Batteries by Electrochemical Impedance Spectroscopy. I. Experimental Investigation,” *Journal of Power Sources*, 196(12), pp. 5334–5341.
- [25] Waag, W., Käbitz, S., and Sauer, D. U., 2013, “Experimental Investigation of the Lithium-Ion Battery Impedance Characteristic at Various Conditions and Aging States and Its Influence on the Application,” *Applied Energy*, 102, pp. 885–897.
- [26] Buller, S., Thele, M., Doncker, R. D., and Karden, E., 2003, “Impedance-Based Simulation Models of Supercapacitors and Li-ion Batteries for Power Electronic Applications,” 38th IAS Annual Meeting on Conference Record of the Industry Applications Conference, 2003.
- [27] Thackeray, M. M., Wolverton, C., and Isaacs, E. D., 2012, “Electrical Energy Storage for Transportation—Approaching the Limits of, and Going beyond, Lithium-Ion Batteries,” *Energy & Environmental Science Energy Environ. Sci.*, 5(7), p. 7854.
- [28] “Basics of Electrochemical Impedance Spectroscopy,” Available: <http://www.gamry.com/application-notes/eis/basics-of-electrochemical-impedance-spectroscopy/>.

- [29] Tarascon, J.-M., and Armand, M., 2001, “Issues and Challenges Facing Rechargeable Lithium Batteries,” *Nature*, 414(6861), pp. 359–367.
- [30] Xu, G.-L., Wang, Q., Fang, J.-C., Xu, Y.-F., Li, J.-T., Huang, L., and Sun, S.-G., 2014, “Tuning the Structure and Property of Nanostructured Cathode Materials of Lithium Ion and Lithium Sulfur Batteries,” *J. Mater. Chem. A*, 2(47), pp. 19941–19962.
- [31] Metrohm, 2011, “Electrochemical Impedance Spectroscopy (EIS) Part 3 – Data Analysis” Available: http://www.ecochemie.nl/download/applicationnotes/autolab_application_note_eis03/.
- [32] German, F., Hintennach, A., Lacroix, A., Thiemig, D., Oswald, S., Scheiba, F., Hoffmann, M. J., and Ehrenberg, H., 2014, “Influence of Temperature and Upper Cut-off Voltage on the Formation of Lithium-ion Cells,” *Journal of Power Sources*, 264, pp. 100–107.
- [33] “Charging Lithium-Ion Batteries,” – Battery University. Available: http://batteryuniversity.com/learn/article/charging_lithium_ion_batteries.
- [34] Deng, D., 2015, “Li-ion batteries: Basics, Progress, and Challenges,” *Energy Science & Engineering Energy Sci Eng*, 3(5), pp. 385–418.
- [35] “BU-802c: How Does Premature Voltage Cut-off Affect the Runtime?,” Premature Voltage Cut-off. Available: http://batteryuniversity.com/learn/article/premature_voltage_cut_off.
- [36] Vable, M., *Mechanics of Materials: Stability of Columns*, and 11, 2014, “STABILITY OF COLUMNS,” *STABILITY OF COLUMNS*, pp. 496–528.
- [37] “Euler's Column Formula,” Euler's Column Formula. Available: http://www.engineeringtoolbox.com/euler-column-formula-d_1813.html.

- [38] Udomphol, T., “Laboratory 7: Bending Test,” Mechanical Metallurgy Laboratory 431303, pp. 1–6.
- [39] Wang, W., Roubier, N., Puel, G., Allain, J.-M., Infante, I., Attal, J.-P., and Vennat, E., 2015, “A New Method Combining Finite Element Analysis and Digital Image Correlation to Assess Macroscopic Mechanical Properties of Dentin,” *Materials*, 8(2), pp. 535–550.
- [40] Mujika, F., 2005, “On the Difference between Flexural Moduli Obtained by Three-Point and Four-Point Bending Tests,” *Polymer Testing*, 25(2), pp. 214–220.
- [41] Berg, S., Akturk, A., Kammoun, M., and Ardebili, H., *in preparation*, “Investigation of the Contact Pressure in Polymer Based Flexible Batteries under Various Bending and Interface Conditions,” pp. 1–13.

